Title:

Perturbed DNA methylation by sustained overexpression of Gadd45b induces chromatin disorganization, DNA strand breaks and dopaminergic neuron death in mice

Authors:

Camille Ravel-Godreuil[1], Olivia Massiani-Beaudoin[1], Philippe Mailly[2], Alain Prochiantz[1], Rajiv L. Joshi[1*] and Julia Fuchs[1*]

Affiliations:

[1]Centre for Interdisciplinary Research in Biology (CIRB), Collège de France, INSERM U1050/ CNRS UMR 7241, PSL Research University, 11 place Marcelin Berthelot, 75231 Paris Cedex 05, France.

[2]Orion Imaging Facility, Center for Interdisciplinary Research in Biology (CIRB), College de France, CNRS Unité Mixte de Recherche 724, INSERM Unité 1050, Labex Memolife, PSL Research University, Paris, France

*For correspondence:

J.F. (Julia.fuchs@college-de-france.fr); R.L.J. (rajiv.joshi@college-de-france.fr)

Abstract

Heterochromatin disorganization is a key hallmark of aging and DNA methylation state is currently the main molecular predictor of chronological age. The most frequent neurodegenerative diseases like Parkinson disease and Alzheimer's disease are age-related but how the aging process and chromatin alterations are linked to neurodegeneration is unknown. Here, we investigated the consequences of viral overexpression of *Gadd45b*, a multifactorial protein involved in active DNA demethylation, in the midbrain of wild-type mice. *Gadd45b* overexpression induces global and stable changes in DNA methylation, particularly on gene bodies of genes related to neuronal functions. DNA methylation changes were accompanied by perturbed H3K9me3-marked heterochromatin and increased DNA damage. Prolonged *Gadd45b* expression resulted in dopaminergic neuron degeneration accompanied by altered expression of candidate genes related to heterochromatin maintenance, DNA methylation or Parkinson disease. *Gadd45b* overexpression rendered midbrain dopaminergic neurons more vulnerable to acute oxidative stress. Heterochromatin disorganization and DNA demethylation resulted in derepression of mostly young LINE-1 transposable elements, a potential source of DNA damage, prior to *Gadd45b*-induced neurodegeneration. Our data implicate that alterations in DNA methylation and heterochromatin organization, LINE-1 derepression and DNA damage can represent important contributors in the pathogenic mechanisms of dopaminergic neuron degeneration with potential implications for Parkinson disease.

Introduction

Epigenetic marks separate chromatin into actively transcribed euchromatin and repressive heterochromatin domains, and participate in the spatial organization of the genome into highly structured 3D domains [1]. These epigenetic signatures include DNA methylation, various post-translational modifications of histones, and attraction forces between different types of genomic repeat elements, including transposable elements (TEs) [1]. Changes in chromatin structure regulate DNA accessibility to transcription factors and the physical proximity of enhancers to promoters, thereby regulating gene expression.

It is well established that DNA methylation regulates various important cellular processes during development and cell differentiation. In recent years, however, perturbations of chromatin organization have been linked to the aging process and global changes in DNA methylation are currently the main molecular predictor of chronological age (reviewed in [2]). Aging-induced epigenetic remodeling of chromatin can impact on genomic stability [3,4,] and vice versa [2]. Thus chromatin states and genomic stability are important, interdependent factors associated with the aging process [5]. One emerging culprit related to both processes is the un-silencing of transposable elements (TEs) with age. Around half of the human genome is comprised of TEs. The evolutionary most successful TEs in mammals are long interspersed nuclear element-1 (LINE-1 or L1). Mostly fossilized and a few remaining active LINE-1 sequences (around 100 in humans and 3000 in mice) represent around 17% of the human [6] and 21% of the mouse genome [7]. Young and full-length LINE-1 elements are autonomous retrotransposons, expanding in the genome through a “copy and paste” retrotransposition mechanism and encoding the two necessary proteins, namely ORF1p and ORF2p, required for their mobilization. ORF1p is an RNA binding protein with strong “cis” preference [8-10] and ORF2p encodes an endonuclease and a reverse transcriptase [11,12]. Several repressive cellular mechanisms, including DNA methylation and heterochromatinization, limit their expression [13]. When these fail with age, TEs can become derepressed [14]. An increased activity of LINE-1 is associated with genomic instability through the induction of DNA damage [15-18] .

How aging and neurodegeneration are linked at the molecular level remains widely unknown. This question is, however, of high relevance as age is the primary

risk factor for the most common neurodegenerative diseases (NDs) including Parkinson disease (PD) and Alzheimer disease (AD) [19]. Some of the cellular processes defined as the hallmarks of aging [20] overlap with pathways shown to be dysfunctional in NDs. This is the case for impaired proteostasis, mitochondrial dysfunction, deregulated nutrient sensing, increased oxidative stress and neuroinflammation [21,22]. Whether two other important nominators of aging, namely perturbations in the organization of chromatin and genomic instability, are associated with neuronal aging and neurodegeneration is not unequivocally proven yet.

A cardinal feature of PD is the degeneration of midbrain dopaminergic (mDA) neurons in the substantia nigra *pars compacta* (SNpc). These neurons project to the striatum and their loss leads to a striatal dopamine deficiency inducing the typical motor symptoms of PD. Decreased global DNA methylation with age in the SNpc has been observed [23] and DNA methylation changes, mostly on specific genetic risk loci, have been linked to several NDs [24] including PD [25]. Alterations in histone modifications have also been observed in PD [26]. However, the possible contribution of age-related epigenetic alterations to the pathogenesis of PD and the onset of neurodegeneration has not been demonstrated yet.

Here, we investigated how SNpc mDA neurons react to perturbations of chromatin organization. For this purpose, we overexpressed *Gadd45b* in the SNpc of wild-type mice using an adeno-associated virus (AAV) vector. GADD45B is a multifunctional protein which coordinates in the nucleus an active DNA demethylation pathway involving cytidine deaminases and DNA glycosylases [27] in association with the base excision repair (BER) pathway [28]. We chose GADD45B because it is a known DNA demethylase in postmitotic neurons [27,29] and it is highly inducible in conditions of oxidative stress in the SNpc [30]. We show that overexpression of *Gadd45b* in the SNpc of wild-type mice leads to widespread perturbations of DNA methylation, heterochromatin disorganization, increased vulnerability to oxidative stress of mDA neurons, activation of LINE-1 elements, DNA strand breaks and neuronal death. Our data reinforces the hypothesis that aging-induced global chromatin disorganization initiates neurodegeneration, possibly via the derepression of LINE-1 elements.

114 ***Results***

115

116 *Gadd45b overexpression in the SNpc of wild-type mice leads to early and stable*
117 *DNA methylation perturbations in gene bodies of genes related to neuronal functions*

118 Wild-type mice littermates (6 weeks old) were injected unilaterally in the SNpc
119 using AAV8-*mCherry* or AAV8-*mGadd45b*. The animals were sacrificed after 14 or
120 90 days *post-injectionem* (p.i.) and either perfused or dissected as schematized in
121 **Figure 1A**. The AAV8-mCherry control virus efficiently infected tyrosine hydroxylase
122 positive (TH+) neurons of the SNpc as shown by mCherry expression at 14d p.i. (***Fig.***
123 ***1B, upper panel***). Due to the lack of a good antibody against GADD45B, expression
124 of *Gadd45b* was verified at 14d p.i. by *in situ* hybridization (***Fig1. B, lower panel***)
125 and RT-qPCR after manual micro-dissection of the SNpc at 14d and 90d p.i. (***Fig.***
126 ***1C***). *Gadd45b* transcripts on the injected ipsilateral side were increased up to 79-fold
127 on average (11.02±4.83; 869.1±283; n=6) at 14d p.i. and up to 178-fold (7.89±1.52;
128 1402±683; n=4) at 90d p.i. compared to the endogenous transcript levels of the non-
129 injected contralateral side.

130 Having verified the efficient overexpression of *Gadd45b* in the SNpc, we asked
131 whether this perturbs DNA methylation patterns in the SNpc. To this end, we injected
132 wild-type mice with AAV8-m*Gadd45b* (n=6) or AAV8-*mCherry* (n=6) and
133 simultaneously extracted DNA and RNA from manually micro-dissected SNpc
134 biopsies at 14d p.i. (***Scheme Fig. 1A***). The DNA of two mice per condition, selected
135 for high expression by RT-qPCR of *Gadd45b* or *mCherry*, respectively, was then
136 subjected to reduced representation bisulfite sequencing (RRBS) for DNA
137 methylation analysis. Bioinformatic analysis of RRBS data detected 809117 CpGs
138 that were common between both conditions. Of those, 76185 individual CpGs were
139 differentially methylated (DMCs) with a q-value smaller than, or equal to, 0.01 and at
140 least 25% difference. Using a window and step size of 1000 bp, differentially
141 methylated regions (DMRs) were defined and 16702 regions passed the defined
142 significance threshold. A majority of DMCs and DMRs was hypomethylated
143 throughout time, located in open sea regions (defined as regions outside CpG
144 islands, CpG shores or CpG shelves) and localized in gene bodies, particularly
145 introns. The Volcano plot in ***Figure 1D*** illustrates the DMC methylation pattern 14d
146 p.i.. Upon *Gadd45b* overexpression, 46508 DMCs (61.05 %) were hypomethylated
147 and 29677 DMCs (38.95%) were hypermethylated. The percentage of hypo- and

148 hypermethylated regions per chromosome was similar (***Suppl. Fig. 1G***). We then
149 interrogated DMCs in relation to their distance to a CpG island and found 69.73% to
150 be overlapping with open sea regions (***Fig. 1E***), defined as regions outside of a
151 known CpG island, CpG shore (2000 bp flanking the CpG island) or CpG shelves
152 (2000 bp flanking the CpG shores). Analysis of the genomic context revealed that
153 41.36% of DMCs were located in introns (***Fig. 1F***), followed by 22.3% in the
154 intergenic space, 23.6% in exons and 12.5% in promoter regions. This analysis
155 indicates early and widespread methylation changes primarily in gene bodies upon
156 *Gadd45b* overexpression.

157 In order to understand the long-term changes in methylation patterns induced
158 by *Gadd45b* overexpression, we extracted DNA from mice 90 days after injection of
159 AAV8-*mGadd45b* or AAV8-*mCherry* control. Analysis revealed a similar distribution
160 of hypo- and hypermethylated DMRs at 14d p.i. (***Suppl. Fig. 1A***) and at 90d p.i.
161 (***Suppl. Fig. 1C***). The genomic context of DMCs and DMRs, both at 14d p.i. (***Suppl.***
162 ***Fig. 1B***) and at 90d p.i. (***Suppl. Fig. 1D***) was very similar as well, the majority of
163 differential methylation concerning open sea regions and gene bodies, particularly
164 introns (summarized in ***Table 1***). The overall numbers of DMRs and DMCs with
165 AAV8-m*Gadd45b* also resembled that at 14d p.i., but common DMRs or DMCs
166 examination revealed an overlap of only 15% of DMRs (2517) and 18% of DMCs
167 (13920) (***Fig. 1G***). While this indicates that the specific regions with methylation
168 changes induced by *Gadd45b* overexpression are not stable over time, the general
169 location in open sea regions and in introns of genes of DMRs and DMCs is
170 maintained as a specific and stable footprint of *Gadd45b* overexpression, which we
171 termed "*Gadd45b*-regulon". Furthermore, there was an important overlap of more
172 than half of the genes containing intronic hypomethylated or hypermethylated DMCs
173 at 14d and at 90d (***Fig. 1H***). The extent of overlap was similar for intronic DMRs
174 (hypoDMRs at 14d: 3937 genes; hypoDMRs at 90d: 3467 genes, overlap (1712
175 common genes); ***Suppl. Fig. 1E***). Of those common genes, 2353 genes contained at
176 least one intronic hypo- and one intronic hypermethylated DMC (***Fig. 1H***) and 447
177 genes at least one intronic hypo- and one intronic hypermethylated DMR at both 14d
178 and 90d p.i. (***Suppl. Fig. 1E***). Thus, *Gadd45b* overexpression induces stable
179 changes in methylation patterns in gene bodies, particularly introns.

180 The results of the RRBS analysis prompted us to identify functional categories
181 associated with this GADD45B-induced methylation footprint corresponding to the

182 2353 genes stably containing DMCs over time (***Fig. 1H***). We used Gene ontology
183 analysis (PANTHER version 15.0; http://pantherdb.org) and the PANTHER
184 overrepresentation test with the GO-Slim annotation data set 'biological process'. 145
185 GO categories were significantly overrepresented with a fold change >2 and an FDR
186 <0.05. The first fifteen significantly overrepresented GO categories are displayed in
187 ***Figure 1I***. Of those, 10 GO categories are explicitly related to neuronal functions with
188 two prevailing categories, namely synaptic function and organization, and
189 neurodevelopment and neurogenesis. This is very similar to what we found for DMRs
190 (***Suppl. Fig. 1F***) and suggests that *Gadd45b* is involved in the specific regulation of
191 gene body methylation of neuron-related genes.
192
193 *Gadd45b overexpression leads to heterochromatin disorganization in mDA neurons*
194 Members of GADD45 protein family have been described to promote
195 heterochromatin relaxation [31]. We therefore examined whether *Gadd45b*
196 overexpression, in addition to global methylation changes, would also alter chromatin
197 organization, in particular the organization of heterochromatin. To do so, we stained
198 mDA neurons for histone H3 lysine 9 trimethylation (H3K9me3), a repressive
199 heterochromatin mark. Immunostaining for H3K9me3 shows a perinucleolar pattern
200 composed, on average, of 3 or 4 foci (3.64±0.12) in TH+ neurons in the SNpc of
201 AAV8-*mCherry* injected mice (***Fig. 2A***). This pattern becomes disorganized in AAV8-
202 *mGadd45b* injected mice at 14d p.i.. Semi-automated quantification of H3K9me3
203 staining specifically in TH+ neurons identified a 1.13-fold increase in the number of
204 H3K9me3 foci (4.10±0.12) scattered across the nucleus, an increase by 1.24-fold of
205 the average H3K9me3 foci volume (4.78±0.15; 5.91±0.22 μm^3), a reduction by 1.21
206 fold in the intensity of the diffuse nucleoplasmic H3K9me3 staining
207 ($2.37x10^7$±557961; $1.96x10^7$±441292), but no difference in foci intensity
208 ($1.32x10^6$±54236; $1.41x10^6$±64942) (***Fig. 2A***, quantification in ***Fig. 2B-E***). This shift in
209 heterochromatin organization is still detectable at 90d p.i. (***Fig. 2F-J***). These results
210 show that a de-structuration of heterochromatin is already detectable 14d and stable
211 up to 90d after the injection of AAV8-*mGadd45b* indicating an early and stable
212 perturbation of global heterochromatin organization upon *Gadd45b* overexpression.
213 We next examined whether *Gadd45b* overexpression leads to perturbations in
214 the pattern of the DNA methylation marker MeCP2. Immunostaining of sections from
215 mice injected with AAV8-*mGadd45b* or AAV8-*mCherry* did not show any difference in

216 the number of MeCP2 foci in TH+ neurons (***Suppl. Fig. 2A-D***), the intensity of the
217 diffuse nucleoplasmic MeCP2 staining nor the volume and intensity of MeCP2 foci,
218 neither at 14d nor at 90d p.i. (***Suppl. Fig. 2E,G-J***). There was a slight increase in foci
219 intensity at 14d p.i. with AAV8-*mGadd45b* (***Suppl. Fig. 2F***). This analysis indicates
220 that DNA methylation perturbation as detected by RRBS does not imply a global
221 change in the organization of MeCP2 distribution.
222
223 *Gadd45b overexpression leads to the loss of TH+ neurons*
224 To examine the effect of *Gadd45b* overexpression on the survival of mDA
225 neurons in the SNpc, we quantified the number of TH+ neurons in mice injected with
226 AAV8-*mCherry* or AAV8-*mGadd45b* at 14d and 90d p.i. (***Fig. 3A***). There was no
227 difference between TH+ cell numbers comparing AAV8-*mCherry*- and AAV8-
228 *mGadd45b*-injected (ipsilateral) sides to the non-injected side (contralateral) at 14d
229 p.i. (***Fig. 3B***: AAV8-*mCherry* ipsi/contra: 1.04±0.02; AAV8-*mGadd45b* ipsi/contra:
230 0.97±0.04). However, 90d after injection of AAV8-*mGadd45b*, this ratio shifted to an
231 average of 0.82±0.04, indicating a specific loss of 18% of TH+ neurons on the AAV8-
232 m*Gadd45b* injected side compared to the contralateral side (***Fig. 3C***). The TH+
233 neurons ratio between the ipsi- and the contralateral side remained unchanged in
234 AAV8-*mCherry* injected mice (***Fig. 3C***: ipsi/contra: 0.97±0.02). These results show
235 that *Gadd45b* overexpression in the SNpc can trigger degeneration of mDA neurons
236 in the long-term. In addition, the absence of a significant TH+ cell loss at 14d p.i.
237 suggests that alterations in the distribution of methylation at CpGs and in the
238 organization of chromatin precede neuronal death.
239
240 *Enhanced vulnerability of mDA neurons overexpressing Gadd45b to oxidative stress*
241 To examine whether the heterochromatin de-structuration observed in TH+
242 neurons at 14d p.i. upon *Gadd45b* overexpression could render these neurons more
243 vulnerable to oxidative stress, mice were first injected with AAV8-*mCherry* or AAV8-
244 *mGadd45b* and 14d later with 6-hydroxy-dopamine (6-OHDA, 2 μl; 0.5 μg/μl) in the
245 ipsilateral striatum. When injected into the striatum, 6-OHDA induces a specific and
246 retrograde death of mDA neurons in the SNpc and is frequently used to model PD in
247 rodents [32] including mice [33]. Three days after the unilateral, striatal injection of 6-
248 OHDA, immunostainings of striatal sections show a 29% loss (mCherry ipsi/contra:
249 0.71±0.04) of TH intensity in the ipsilateral striatum compared to the contralateral

250 side in mCherry expressing mice (illustrated in ***Fig. 3D,*** *quantified in* ***Fig. 3E, left***
251 ***panel***). This decrease in TH staining intensity reaches 44% (mGadd45b ipsi/contra:
252 0.56±0.04) in AAV8-*mGadd45b* injected mice (***Fig. 3D, right panel***), suggesting that
253 *Gadd45b* overexpression increases the axonal degeneration of mDA neurons
254 induced by 6-OHDA. However, this experimental paradigm did not lead to any
255 significant loss of TH cell bodies in the SNpc (***Fig. 3F***), potentially due to the time of
256 analysis. We analyzed mice 3 days rather than 6 days after 6-OHDA injection, the
257 time point normally used to induce mDA cell death in the SNpc [32], to identify early
258 events in TH+ cell bodies. An increased vulnerability to oxidative stress of mDA
259 neurons overexpressing *Gadd45b* was also reflected at the heterochromatin level.
260 The injection of 6-OHDA changed the nuclear localization and increased the number
261 of H3K9me3 positive foci (***Fig. 3G, H)*** compared to AAV8-*mCherry*. Under these
262 conditions, the number of MeCP2 positive foci in mDA neurons expressing AAV8-
263 *mGadd45b* was also increased as compared to AAV8-*mCherry* (***Fig. 3I, J***). This
264 presumably reflects more significant DNA methylation changes upon *Gadd45b*
265 overexpression under oxidative stress.
266
267 *Chromatin de-structuration is accompanied by increased DNA damage*
268 The heterochromatin loss model of aging stipulates that heterochromatin de-
269 condensation is a driving force of cellular aging [34]. Loss of proteins involved in
270 heterochromatin maintenance has been shown to lead to increased DNA damage
271 and accelerated aging [35,36] . In the context of NDs, recent studies have reported that
272 chromatin relaxation in the brain could also result in increased DNA damage and
273 genome instability [18,37-39]. Since *Gadd45b* overexpression led to chromatin changes,
274 we investigated whether it might also induce DNA damage. We therefore performed
275 immunostainings for phosphorylated histone H2AX (γ-H2AX), a marker for DNA
276 strand breaks (***Fig. 4A***). TH+ neurons contained either a single perinucleolar focus or
277 a diffuse nucleoplasmic staining without any foci. After injection of AAV8-*mGadd45b*
278 (14d p.i.), the majority (65.94±2.10 %) of TH+ neurons displayed a diffuse, intense
279 nucleoplasmic staining against only 39.81±2.40 % of TH+ neurons after AAV8-
280 *mCherry* injection, the majority showing one or more prominent perinucleolar γ-
281 H2AX-positive foci (***Fig. 4B, C***). The quantification of the diffuse γ-H2AX staining in

282 the nucleus revealed a more intense staining after *Gadd45b* overexpression,
283 indicating widespread DNA damage.
284
285 *LINE-1 methylation is affected by Gadd45b overexpression*
286 Heterochromatin alterations can unsilence normally repressed TEs, including
287 LINE-1 elements [14]. LINE-1 are a potential source of DNA damage [16-18,40]. Repeat
288 elements are detected by RRBS and the Bismark software used for mapping of the
289 RRBS reads only considers uniquely mapped reads to avoid any bias during the
290 methylation calling. Thus, reads that are mapping with a same mapping score to
291 multiple locations on the reference genome, which will be the case for most reads
292 derived from repetitive elements, will not be considered. We exploited these facts to
293 explore the methylation status of LINE-1 elements in our experimental conditions.
294 Using the RRBS data, we used the LINE-1 annotation included in the software
295 HOMER, which contains its own database of LINE-1 elements for the mouse genome
296 to interrogate the overlap of DMRs and DMCs with LINE-1 elements 14 days after
297 injection of AAV8 viruses. This analysis showed that 3530 DMCs and 1030 DMRs
298 overlapped with an annotated LINE-1 element, which we termed L1-DMCs and L1-
299 DMRs respectively. 794 (22.5%) L1-DMCs (***Fig. 5A***) and 264 (25.6%) L1-DMRs
300 (***Suppl. Fig. 3A***) were located in intronic regions, and 2734 (77.5%) L1-DMCs (***Fig.***
301 ***5A***) and 766 L1-DMRs (***Suppl. Fig. 3A***) in intergenic regions. Of all L1-DMCs the
302 majority was hypomethylated (1933, 54,8%, ***Fig. 5B***), similar to L1-DMRs (595,
303 57,8%).
304
305 To determine which LINE-1 families containing at least one L1-DMC upon
306 *Gadd45b* overexpression were overrepresented, we counted the number of families
307 and ordered them by frequency. ***Figure 5C*** shows the ten most represented LINE-1
308 families with a L1-DMC. Interestingly, of 94 different families present, three LINE-1
309 family members, namely L1-MdF2 (975 L1-DMCs), L1Md-T (349 L1-DMCs) and
310 L1Md-A (280 L1-DMCs), were the three most frequently represented. L1Md-T, L1Md-
311 A and L1-Md_F2 elements are young LINE-1 elements [41], which contain full-length,
312 retrotransposition-competent LINE-1 copies. Of LINE-1 associated intronic DMCs
313 (L1-iDMCs, 794) at 14d p.i., the majority (54.7%) was hypomethylated (434
314 hypomethylated vs 360 hypermethylated, ***Fig. 5D***). L1-iDMCs were mostly located in
315 protein-coding genes (82.8%, ***Fig. 5E***) and the GO analysis of biological processes

316 of 483 genes, containing at least one L1-iDMC, identified seven enriched categories.
317 Among those categories, three were neuron-related (***Fig. 5G***). The most frequent
318 LINE-1 families in intronic L1-iDMCs were, again, the young L1Md-F2 family (139 of
319 794) and L1Md-T (57 L1-iDMCs) followed by the old Lx8 family (57 L1-iDMCs) (***Fig.***
320 ***5F***). Notably, other young LINE-1 families were also overlapping with iDMCs (L1Md-
321 A: 27 L1-iDMCs, L1Md-Gf: 6 L1-iDMCs, not shown) (***Fig. 5F***). Similarly to L1-iDMCs,
322 the majority of LINE-1 associated DMRs in introns (L1-iDMRs) was hypomethylated
323 (63,3 %, 167 L1-iDMRs; ***Suppl. Fig. 3A***) and belonged to the L1Md-F2 family (39 of
324 264) (***Suppl. Fig. 3B***). Hypo- and hypermethylated iDMRs were also found in LINE-1
325 elements of the active L1Md-T (3 and 2, respectively) and L1Md-A families (3 and 3
326 elements, respectively). This prompted to examine a data-base annotating full-length
327 LINE-1 elements (L1Basev2 [42]) to see if intronic and intergenic DMRs and DMCs
328 could coincide with possibly active LINE-1. Ten DMRs and 62 DMCs overlapped with
329 a full-length LINE-1. More than half of them (7 out of 10 DMRs and 38 out of 62
330 DMCs, ***Fig. 5H, Suppl. Fig. 3C)***, were hypomethylated. This data indicates a
331 widespread change in the methylation status of LINE-1 elements upon *Gadd45b*
332 overexpression (14d p.i.). The most differentially methylated LINE-1 elements are
333 hypomethylated and belong to young L1 families (L1Md-F2, L1Md-T, L1Md-A)
334 suggesting a possible expression of these individual LINE-1 loci. Interestingly, L1-
335 iDMCs are frequently located in introns of genes related to neuronal functions.
336
337 *LINE-1 transcripts are increased upon overexpression of Gadd45b*
338 Having established a change in the methylation pattern of LINE-1 elements
339 after injection of AAV8-*mGadd45b*, some of which were full-length, we evaluated the
340 expression of the youngest L1 families in mice, namely L1Md-A and L1Md-Tf/Gf. The
341 analysis by RT-qPCR with specific primers located in the 5'UTR of the L1Md-A (***Fig.***
342 ***5I, left panel***) and L1Md-Gf/Tf families (***Fig. 5I, right panel***) showed a 1.5-fold
343 increase in LINE-1 transcripts in the SNpc after 14d of *Gadd45b* overexpression.
344
345 *Gadd45b overexpression is accompanied by expression changes in genes with*
346 *DMCs*
347 Expression levels of candidate genes with intronic DMCs at either 14d or 90d
348 p.i. were then analyzed by RT-qPCR. We selected 13 genes based on their known
349 function either in chromatin remodeling (*Satb1*, *Setdb1, Wapl*), DNA methylation

350 (*Tet2*, *Tet3, Dnmt3a*), PD relevance (*Lrrk2, Park2*), synaptic remodeling (*Sorcs2*),
351 DNA damage (*Xpa*), or in aging and senescence (*Cdkn2a-p19, Cdkn2d, Sirt1)*. None
352 of the candidate genes showed a change in expression at 14d p.i. However, at 90d
353 p.i., the expression of *Satb1*, *Setdb1*, *Dnmt3a*, *Tet3* and *Park2* decreased
354 significantly in the ipsilateral SNpc injected with AAV8-*mGadd45b* compared to
355 AAV8-*mCherry*. (***Fig. 6A***). Of note, 4 out of these 5 are genes belonging to the
356 *Gadd45b*-DMC-regulon (***Fig. 1H***). Using RNA-seq data of laser-microdissected SNpc
357 from wild-type mice (GEO *GSE72321;* [30] and unpublished), we compared the
358 expression levels of the selected candidate genes to those of dopaminergic neuron-
359 specific markers such as *TH*, dopamine transporter *Slc6a3* or the homeogene,
360 *Engrailed* 1 (*En1*)[43]. We found high levels of expression of *Satb1* compared to the
361 other selected genes, indicating that *Satb1* is strongly expressed in the SNpc (***Suppl.***
362 ***Fig. 4***). Exonic and intronic DMCs over downregulated genes comprised hypo- as
363 well as hypermethylated CpGs. Disruption of the normal gene body methylation state
364 of several genes of the GADD45B-DMC-regulon might thus provoke their
365 dysregulation over time but is not associated with a loss of a particular methylation
366 pattern.

367 ***Discussion***

368

369 Epigenetic alterations and chromatin relaxation are hallmarks of aging [2,3], but
370 evidence of age- and disease-related global changes in the epigenetic landscape of
371 different neuronal populations is still scarce. This information, however, holds
372 important promises for understanding the implication of aging in the neuronal
373 degeneration characterizing age-related NDs and might thus foster the
374 understanding of the pathogenesis of NDs.

375 Here, we show that *Gadd45b* overexpression induces early changes in DNA
376 methylation, particularly in introns of genes related to neuronal functions and on
377 young and potentially active LINE-1 elements. This, accompanied by perturbations of
378 heterochromatin organization and increased DNA damage culminate in neuronal cell
379 death after several weeks. At an early time point before the onset of
380 neurodegeneration, *Gadd45b* overexpression induces a vulnerable state in mDA
381 neurons, increasing their sensitivity to oxidative stress induced by the striatal
382 injection of 6-OHDA. This vulnerability is characterized by an amplified striatal
383 dopaminergic axon terminal loss and an accentuation of perturbations in the
384 organization of heterochromatin and DNA methylation in mDA cell bodies of the
385 SNpc. We also demonstrate that LINE-1 transcripts are increased early on after
386 *Gadd45b* overexpression. This increase in LINE-1, which are potent inducers of DNA
387 damage in mDA neurons [18], could explain the cell death of mDA neurons we observe
388 when overexpressing *Gadd45b* long-term.

389 A number of recent studies indicate that GADD45 proteins play a key role in
390 active DNA demethylation in post-mitotic neurons in the brain [27,28] by serving as
391 scaffolding proteins to recruit DNA repair enzymes such as the thymidine DNA
392 glycosylase (TDG) to the site of DNA demethylation [44]. So far, GADD45B-regulated
393 DNA demethylation has been described in the context of adult neurogenesis [29],
394 depressive-like behavior in mice [45], major psychosis in humans [46] and cerebral cortex
395 plasticity [47] on specific promoters, mostly on promoters of the *Bdnf* gene.
396 Unexpectedly, when overexpressing *Gadd45b* in the SNpc of wild-type mice, we
397 observed very limited changes in methylation on gene promoters, but rather
398 widespread methylation changes on gene bodies with both, hypermethylated and
399 hypomethylated CpGs. This apparent discrepancy with previous studies in terms of
400 extent, localization and pattern of the DNA methylation changes induced by

401 GADD45B might be due to methodology. Indeed, most studies in the brain did not
402 use techniques allowing for unbiased global DNA methylation surveillance.
403 GADD45B has been shown to associate with TET (Ten-eleven translocation)
404 proteins [48,49] which transform 5-methylcytosines (5mC) through a series of sequential
405 oxidations. Those modified cytosines are excised by TDG and then replaced by non-
406 methylated cytosines through BER-dependent mechanisms [50]. A recent study has
407 shown that *Tet2* expression is increased in PD patients leading to altered 5mC
408 patterns in enhancers of neuronal genes. Conversely, TET2 loss in mDA neurons
409 was neuroprotective [51]. *Tet2* did not show any changes in expression at either time
410 point after AAV8-*mGadd45b* injection. This might be explained by the fact that *Tet2*
411 has many splice variants, which were not all covered in our RT-qPCR assay.
412 However, *Tet3* is down-regulated 90d after AAV8-*mGadd45b* injection. TET3 has
413 been shown to interact with transcriptional regulators and histone writers such as
414 H3K36 methyltransferases and to allow the active transcription of certain neuronal
415 genes [52]. TET3 has also been reported to bind DNA and prevent aberrant
416 methylation at the transcription start site of genes involved in lysosomal functions,
417 mRNA processing and the BER pathway, pointing to a possible relevance of TET3 in
418 the pathogenesis of NDs [53]. While our knowledge of how genome-wide DNA
419 methylation patterns or epigenetic changes are correlated with PD pathogenesis is
420 still scarce, there is evidence supporting that methylation changes in the SNpc
421 correlate with aging [23] and with cognitive impairment in PD [54]. Most of the existing
422 data concerns methylation patterns of specific genes associated with NDs.
423 Expression of the *SNCA* gene, encoding α-synuclein and mutated in familial PD, for
424 example, is under the control of DNA methylation [55,56]. Chromatin modifications on
425 specific genes have also been reported, and the expression of several genes
426 mutated in PD are modulated by histone modifications, including *SNCA* and *MAPT*
427 encoding Tau [25]. Differentially methylated enhancers have been reported in AD
428 patients, and a dysregulation of histone acetylation in both, AD and PD patients [57-60].
429 By serving as an adaptor between repair factors and chromatin, GADD45B
430 can be seen as a communicating platform between DNA repair and epigenetics [28,61].
431 This could provide an explanation to the fact that we observe global changes in
432 heterochromatin organization in addition to changes in DNA methylation. In line with
433 this, GADD45 proteins have been reported to induce heterochromatin relaxation
434 during cellular reprogramming [31]. GADD45B might thus be part of protein

435 coordinators which link DNA methylation and histone modifications [60]. Perturbations
436 of DNA methylation and global changes in heterochromatin organization, as we show
437 here, induce neurodegeneration of mDA neurons in the SNpc with time and might
438 thus be primary drivers of neurodegeneration.

439 Another primary hallmark of aging is genomic instability and some data
440 suggest that this is also true in neuronal aging [22]. In this context it is important to
441 note, that DNA strand breaks are physiologically occurring in post-mitotic neurons.
442 This physiological process, however, needs to be tightly regulated, since the
443 induction of DNA strand breaks is pathologically exacerbated in AD [62]. We have
444 shown earlier, that DNA damage in mDA neurons can be induced by acute and
445 chronic oxidative stress [18,30] and that LINE-1 activity participates in DNA damage [18].
446 In the latter study, DNA damage was prevented either by siRNA against LINE-1
447 ORF2, the LINE-1 repressive protein Piwil1 or a nucleoside analogue reverse
448 transcriptase inhibitor *in vitro* [18]. This LINE-1 induced DNA damage is dependent on
449 young and active LINE-1 copies. These young LINE-1 elements belong mainly to the
450 L1Md-Tf/Gf, A and F families. In this context it is interesting to note that we observe
451 the most pronounced changes in DNA methylation upon *Gadd45b* overexpression on
452 these young LINE-1 families (***Fig. 5***). Intronic DMCs and DMRs, intronic L1-
453 associated DMCs (L1-iDMCs), and DMCs or DMRs overlapping with full-length LINE-
454 1 (flL1-iDMCs/flL1-iDMRs), are majorly hypomethylated and iDMCs are preferentially
455 located in genes related to neuronal functions. It is therefore conceivable that the
456 changes in methylation patterns we observe upon *Gadd45b* overexpression,
457 particularly on young LINE-1 elements, are functionally linked to the increase in
458 LINE-1 transcripts we observe 14 days after injection of AAV8-*mGadd45b*.
459 Furthermore, based on previous evidence summarized above, this increase in
460 expression of young L1 elements of the L1Md-Tf/Gf, A and F families might be at the
461 origin of the DNA damage in mDA neurons upon *Gadd45b* overexpression.

462 Several lines of evidence suggest that the activation of TEs might be
463 associated with aging and NDs. The expression of LINE-1 in wild-type mice
464 increases in neurons [63], liver and muscle during aging [64]. The activation of TEs with
465 aging leads to neuronal decline and shorter lifespan in drosophila [65,66] and increased
466 TE expression has been reported in brain tissue from PD, AD and ALS patients [37,67].
467 Recently, elevated transcripts of repetitive sequences have been found in the blood
468 of PD patients [68]. Heterochromatin de-structuration and increased TE activity lead to

469 an AD-like phenotype in a mouse model with targeted disruption of *Bmi1*, a gene
470 involved in heterochromatin maintenance and altered expression in AD patients [39]. In
471 AD and in ALS, the Tau protein as well as TDP-43 can induce heterochromatin
472 relaxation, especially at the level of LINE-1 elements in the case of TDP-43, leading
473 to increased TE activity and neurotoxicity [37,67,69]. An aging-induced activation of TEs,
474 which are intrinsic components of the genomes of virtually all eukaryotes, might link
475 genomic instability and epigenetic changes to the aging process.

476 Changes in chromatin states lead to changes in gene expression as
477 exemplified during the transition from neuronal progenitors to adult neurons [70] and
478 during aging [71], and recent data suggests that this could also be the case in NDs
479 [59,72]. In several NDs (AD and HD [73,74]; ALS [75]), disease-specific gene expression
480 changes are increasingly recognized, but whether they overlap with expression
481 profiles characteristic to aging is not known yet. In AD patients, widespread loss of
482 heterochromatin was accompanied by a transcriptomic profile resembling the one of
483 a fetal brain [38], suggesting that the relaxation of chromatin allows the expression of
484 normally repressed genes which alters several biological processes and leads to
485 neurodegeneration neurodegeneration [76]. This is also in line with our data showing
486 the preferential location of iDMCs and iDMRs in genes involved in neurogenesis but
487 it remains to be seen whether their expression is altered. Interestingly, it has been
488 shown that *Gadd45b* activity promotes adult neurogenesis [29]. The majority of these
489 genes with iDMCs and iDMRs upon overexpression of *Gadd45b* belonged to
490 neuronal categories, particularly synapse-related and neurodevelopmental
491 categories. In this context it is interesting to note that synaptic homeostasis is an
492 emerging key player in the pathogenesis of PD [77] and synaptic dysfunction is an
493 early event in neurodegeneration [78]. *Gadd45b* overexpression induced DMCs and
494 DMRs preferentially in introns of genes. The role of gene body or intronic methylation
495 on gene expression is not completely understood [79]. In recent years, several studies
496 have reported that gene body methylation influences gene expression levels and/or
497 alternative splicing [80] [81] [82]. Among the list of genes underlying a direct or indirect
498 regulation through methylation changes triggered by *Gadd45b* overexpression, the
499 decrease in expression did not correlate with a specific direction of methylation
500 changes towards hypo- or hypermethylated CpGs but rather with a change in the
501 methylation state throughout the gene body. *Satb1* has been described as a
502 dopaminergic-specific regulator of senescence [83], a dopaminergic neuron cell

503 survival factor [84] and a regulator of global chromatin structuration [85,86]. The decline in
504 *Satb1* expression at 90d p.i. might help to explain, at least partly, the
505 neurodegeneration of mDA neurons upon *Gadd45b* overexpression. *Setdb1* is a
506 histone-lysine-methyltransferase that specifically trimethylates lysine-9 of histone H3.
507 It is tempting to speculate that the decrease in expression might relate to the change
508 in the organization of H3K9me3 we observe upon *Gadd45b* overexpression. *Dnmt3a*,
509 a genome-wide *de novo* DNA methyltrasferase, and *Tet3*, are involved in DNA
510 methylation or demethylation, respectively. Interestingly, inactivation of TET and/or
511 DNMT proteins causes gains and losses of DNA methylation, suggesting that the
512 loss of one regulator can lead to the redistribution of other regulators and of DNA
513 modifications [87]. *Park2,* encoding the ubiquitin protein ligase Parkin, is a PD-related
514 gene and loss-of-function mutations in this gene are responsible for familial forms of
515 PD. It is thus possible, that a decrease in the expression of *Park2* in the context of
516 *Gadd45b* overexpression might contribute to the degeneration of mDA neurons.
517 Overall, the expression changes might be due to the *Gadd45b*-induced epigenetic
518 dysregulation of the neuronal genome and participate in the *Gadd45b*
519 overexpression phenotype and the challenge will be to correlate one with the other.
520 Altogether, our data are in line with an emerging concept on a new pathogenic
521 pathway initiating age-related neurodegeneration. Recent evidence, including from
522 our group, suggests that aging-induced chromatin reorganization triggers the
523 activation of LINE-1 retrotransposons and subsequent LINE-1 induced DNA damage
524 cumulating in neuronal cell death. Our group has shown that acute and chronic
525 oxidative stress leads to heterochromatin relaxation and LINE-1 activation in mDA
526 neurons *in vivo* [18,30]. Aging-induced epigenetic alterations might produce a vulnerable
527 pre-ND state. Combining this pre-ND state with a particular genetic susceptibility, a
528 familial gene mutation or an accelerating environmental trigger, could initiate a
529 cascade of secondary events including protein aggregation, metabolic dysregulation
530 and mitochondrial dysfunctions. NDs share several common pathological features
531 and despite extensive investigation, no disease-modifying treatment is available.
532 Acknowledging aging as a vulnerability factor for neurodegeneration is important not
533 only for understanding the pathogenesis of NDs, but also for modeling, testing and
534 developing therapeutics for crucially lacking disease-modifying treatments. Our study
535 suggests two novel therapeutic targets for neuroprotection. Drugs restoring

536 chromatin structure and/or repressing LINE-1 transcription or activity might hold
537 promise for the prevention of age-related neurodegeneration.

538 ***Materials and Methods***

539

540 *Animals*

541 All animal treatments followed the guidelines for the care and use of laboratory
542 animals (US National Institutes of Health), the European Directive number
543 2010/68/UE (EEC Council for Animal Protection in Experimental Research and Other
544 Scientific Utilization). This project was validated by the competent ethical committee
545 (CEA 59) and authorized by the Minister of Higher Education, Research and
546 Innovation (n° 00703.01 and n° APAFIS#6605-2016090209434306 v3). For surgical
547 procedures, animals were anesthetized with Xylazine (Rompun 2%, 5 mg/kg) and
548 Ketamine (Imalgene 1000, 80 mg/kg) by intraperitoneal injection and a local
549 subcutaneous injection of lidocaine (0.5%, 3mg/kg) on the incision site. Post-
550 chirurgical analgesia was insured by an injection of the analgesic Meloxicam
551 (Metacam, 0,5mg/kg) s.c.. Swiss OF1 wild-type mice (Janvier) were maintained
552 under a 12 h day/night cycle with ad libitum access to food and water. A maximum of
553 5 mice were housed in one cage, and cotton material was provided for mice to build
554 a nest. Experimental groups consisted of five to seven male mice of 6 weeks of age.
555 Sample size calculations were based on previous experiments.

556

557 *AAV8 vectors to overexpress Gadd45b*

558 Forced expression of *Gadd45b* in mDA neurons was achieved using an AAV8 viral
559 vector. The constructs contained cDNAs for either mouse *Gadd45b* (AAV8-
560 *mGadd45b*) or *mCherry* (AAV8-*mCherry*) under the control of the ubiquitous EF1a
561 promotor. *Gadd45b* cDNA was flanked by the cognate 5' and 3' UTRs (***Fig. 1A***).
562 AAV8 was chosen because it has previously been shown to efficiently infect mDA
563 neurons in the midbrain.

564

565 *Brain injections*

566 For injections, mice were placed in a stereotaxic instrument, and a burr hole was
567 drilled into the skull 3.3 mm caudal and 1.3 mm lateral to the Bregma. The needle
568 was lowered 3.8 mm from the surface of the skull, and AAV8-Ef1a-*mCherry* or AAV8-
569 Ef1a-*mGadd45b* (Vector Biolabs; 2 μl; 4.8×10^{13} GC/ml suspended in NaCl 0,9% with
570 5% glycerol) injections were performed over 4 min. Where indicated 6-OHDA (2 μl;

571 0.5 μg/μl; Sigma) injections were performed in the same manner 0.4 mm rostral, 1.8
572 mm lateral and 3.8 mm ventral to the bregma, over 4 min.
573
574 *Tissue dissection*
575 For RNA and DNA analyses, biopsies of the SNpc were performed. Brains were put
576 into a custom-made brain slicer for adult mice brain. A coronal slice of ≈2mm
577 encompassing the SNpc was excised (Bregma -3.26 mm to -5.2mm) and placed on a
578 cold cover slide with the rostral side facing the experimenter. Dissection of the SNpc
579 was then done following anatomical landmarks: a sagittal cut to separate the two
580 hemisphere, a second parasagittal cut through the fasciculus retroflexus and the
581 mammillothalamic tract (about 2/3 starting from the midline of the distance between
582 the midline and the rostral end of cerebral peduncle) to remove the VTA, a
583 transversal section from the ventral part of the lateral geniculate complex to the
584 midline, a second transversal cut from the ventral end of the cerebral peduncle to the
585 midline. The cerebral cortex was then removed to only keep the midbrain part
586 containing the SNpc and immediately frozen on dry ice and kept at -80°C until
587 extraction.

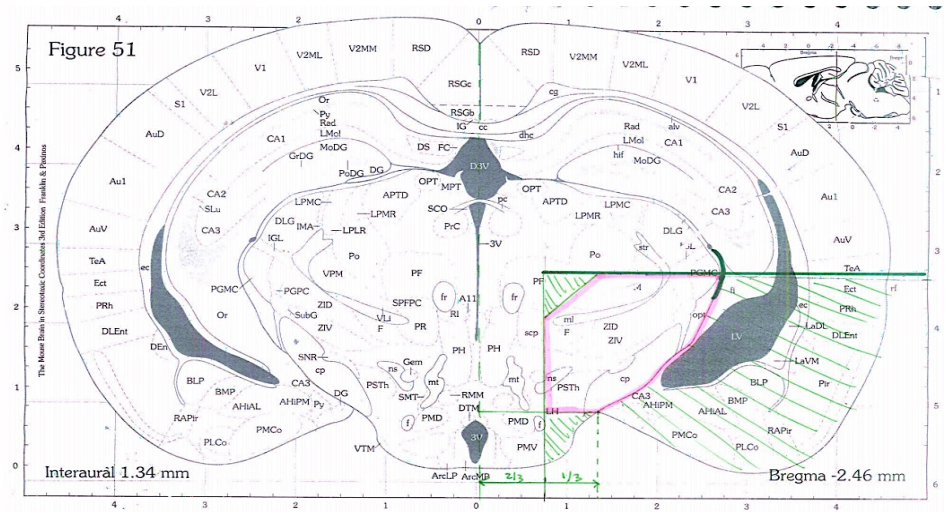

588
589
590 *RT-qPCR*
591 Total RNA from dissected SNpc was extracted using the AllPrep DNA/RNA Micro Kit
592 (Qiagen 80284) adding an on-column DNase I treatment (Qiagen 79256), followed by
593 RT-qPCR. RNA (200 ng) was reverse-transcribed using the QuantiTect Reverse
594 Transcription kit (Qiagen 205313). Quantitative PCR reactions were carried out in
595 duplicates with SYBR Green I Master Mix (Roche S-7563) on a LightCycler 480

596 system (Roche Applied Science). The following primers were used: Hprt (sense:
597 AGCAGGTGTTCTAGTCCTGTGG, antisense: ACGCAGCAACTGACATTTCTAA);
598 LINE-1 A (sense: TTCTGCCAGGAGTCTGGTTC, antisense:
599 TGAGCAGACCTGGAGGGTAG); LINE-1 Tf/Gf (sense:
600 CTGGGAACTGCCAAAGCAAC, antisense: CCTCCGTTTACCTTTCGCCA);
601 Gadd45b (sense: ACTGATGAATGTGGACCCCG, antisense:
602 CCTCTGCATGCCTGATACCC); Satb1 (sense: TCTTTTACCCCCTCCTCCCA,
603 antisense: TCACCTGCCAGAACACTTCA); Tet3 (sense:
604 CTCGGCGGGGATAATGGGAG, antisense: AGCCTGTCTTGACAGTCGCC);
605 Dnmt3a (sense: GCCGAATTGTGTCTTGGTGGATGACA, antisense:
606 CCTGGTGGAATGCACTGCAGAAGGA), Setdb1 (sense:
607 GTTTGCCTGGGTTTGGCAAG, antisense: CTTTGGCCCTCAGTCCGTC); Park2
608 (sense: GCTCAAGGAAGTGGTTGCTAAG, antisense:
609 CAATACTCTGTTGTTCCAGGTCA). Primer efficiencies were tested using 10-fold
610 dilution series of cDNA spanning at least three orders of magnitude. Data were
611 analyzed using the ddCt method and values normalized to hypoxanthine-guanine
612 phosphoribosyl transferase (Hprt).
613
614 *DNA extraction and quantification*
615 DNA was also extracted during the same process of RNA extraction using the
616 AllPrep DNA/RNA Micro Kit (Qiagen 80284). The DNA was then purified, treated with
617 RNase H (ThermoFischer, 18021071) and Proteinase K (PCR grade, Roche,
618 3115836001) and concentrated with the DNA Clean & Concentrator-5 kit (Zymo,
619 D4013). DNA concentration of each sample was measured using the Qubit®
620 fluorometer with dsDNA BR Assay Kit (Thermo Fisher Scientific).
621
622 *RRBS*
623 RRBS was performed by Diagenode. DNA quality of the samples was assessed with
624 the Fragment AnalyzerTM and the DNF-488 High Sensitivity genomic DNA Analysis
625 Kit (Agilent). DNA was slightly more fragmented than defined by the quality control
626 standards but this fragmentation was minor. RRBS libraries were prepared using the
627 Premium Reduced Representation Bisulfite Sequencing (RRBS) Kit (Diagenode)
628 which uses the MspI restriction enzyme and size selection to enrich for CpG-rich
629 regions (coverage of about 4 million CpGs). 100ng of genomic DNA were used to

630 start library preparation for each sample. Following library preparation, samples were
631 pooled together by 8. PCR clean-up after the final library amplification was performed
632 using a 1.45x beads:sample ratio of Agencourt® AMPure® XP (Beckman Coulter).
633 DNA concentration of the pools was measured using the Qubit® dsDNA HS Assay
634 Kit (Thermo Fisher Scientific). The profile of the pools was checked using the High
635 Sensitivity DNA chip for 2100 Bioanalyzer (Agilent). RRBS library pools were
636 sequenced on a HiSeq3000 (Illumina) using 50 bp single-read sequencing (SR50).
637 Bisulfite conversion and amplification were performed using Diagenode's Premium
638 RRBS Kit. After conversion, the pooled samples were analyzed by qPCR.
639 Sequencing was performed in single-end mode, generating 50 bases reads (SE50)
640 on an Illumina HiSeq 3000/4000. Quality control of sequencing reads was performed
641 using FastQC version 0.11.8
642 (https://www.bioinformatics.babraham.ac.uk/projects/fastqc/). Adapter removal was
643 performed using Trim Galore
644 (https://www.bioinformatics.babraham.ac.uk/projects/trim_galore/) version 0.4.1.
645 Reads were then aligned to the murine reference genome mm10/GRCm38 using
646 bismark v0.20.0 [88]. Bismark is a specialized tool for mapping bisulfite-treated reads
647 such as the ones generated in RRBS-seq experiments. Bismark requires that the
648 referenced genome first undergoes an in-silico bisulfite conversion while transforming
649 the genome into forward (C → T) and reverse strand (G → A) versions. The reads
650 producing a unique best hit to one of the bisulfite genomes were then compared to
651 the unconverted genome to identify cytosine contexts (CpG, CHG or CHH - where H
652 is A, C or T). The cytosine2coverage and bismark_methylation_extractor modules of
653 Bismark were used to infer the methylation state of all cytosines (for every single
654 uniquely mappable read) and their context, and to compute the percentage
655 methylation. The reported cytosines were filtered to get only the CpGs covered in
656 each sample. The spike-in control sequences were used at this step to check the
657 bisulfite conversion rates and to validate the efficiency of the bisulfite treatment.
658 Methylkit v1.7.0 [89], a R/Bioconductor package, was used to perform the differential
659 methylation analysis between the two groups of samples. The CpG data set was
660 filtered for low coverage (CpGs with coverage less than 10X in all samples per
661 comparative group were discarded) and for extremely high coverage to discard reads
662 with possible PCR bias (CpGs with coverage higher than the 99.9th percentile were
663 discarded). The data was then normalized for read coverage distribution between

samples. A pairwise comparison was performed for first versus second group of samples to identify differentially methylated CpGs (DMCs) and differentially methylated regions (DMRs), the latter with a window and step size of 1000bp. Methylkit uses logistic regression to compare the methylation percentages between groups at a given CpG/region. All DMCs and DMRs were annotated with the R/Bioconductor package annotation [90], with the refGene and CpG island annotations from UCSC. The annotation comprised two categories: (i) distance to a CpG island and (ii) regional annotation. The distance related annotation classified DMCs and DMRs whether they overlapped a known CpG island, 2000 bp of the flanking regions of the CpG islands (shores), 2000 bp of the flanking regions of the shores (shelves) or outside these regions (open sea). The regional analysis classified DMCs and DMRs in four groups, namely, exons, introns, promoters and intergenic regions.

Sample Name	Total reads	Uniquely aligned	Mapping efficiency (%)	CpGs detected	CpGs cov>10	Average Coverage	Conv. Rate Meth. spike-in (%)	Conv. Rate Unmeth. spike-in (%)
mC1_2w	32.674.187	21.455.193	65.66	1.552.817	1.316.296	36.96	1.76	99.34
mC4_2w	45.583.765	29.506.694	64.73	1.786.123	1.544.593	38.73	1.56	99.53
mG1_2w	39.606.244	26.791.258	67.64	1.727.650	1.495.577	40.53	1.48	99.30
mG6_2w	43.911.896	29.422.323	67.00	1.742.579	1.527.329	43.18	1.56	99.47
mC1_3m	43.426.559	28.584.928	65.82	1.719.287	1.499.415	40.19	1.31	99.51
mC3_3m	37.983.254	24.904.215	65.57	1.644.193	1.412.632	37.57	1.64	99.42
mG1_3m	41.810.446	27.906.101	66.74	1.665.705	1.481.471	44.30	1.73	99.52
mG4_3m	37.699.685	24.957.045	66.20	1.652.248	1.422.694	36.72	1.72	99.47

Immunostaining

For immunostaining, animals received a lethal intraperitoneal injection of 1 µl/g body weight dose of Euthasol (150mg/kg) and were then perfused with 8 mL of Phosphate Buffer Saline (PBS) then 8 mL of 4% Paraformaldehyde (PFA) at a rate of 300 ml/h using a syringe pump. Brains were then post-fixated 1 hour at room temperature (RT) in 4% PFA, washed in PBS three times for 30 minutes at RT and placed in PBS with 20% sucrose overnight at 4°C. After cryoprotection, the brains were embedded in Tissue Freezing Medium (TFM, Microm Microtech), frozen on dry ice and 30 µm sections of mouse striatum and ventral midbrains encompassing the SNpc were prepared using an HM 560 Microm cryostat (Thermo Scientific).

Slides with 30 µm striatum or midbrain sections were washed in PBS and permeabilized with 1% Triton X-100. After 30 minutes at RT in 100 µM glycine buffer (for TH/mCherry and TH/ORF1p) or 30 minutes at 100°C in demasking citrate buffer (10 mM, pH 6, 0.05% Tween) (for TH/MeCP2, H3K9 or γ-H2AX), sections were first

692 blocked in 10% Fetal Bovine Serum (FBS, Gibco) in the presence of 0.5% Triton X-
693 100 for 1 hour at RT and incubated with primary antibodies overnight at 4°C, washed
694 and further incubated with secondary antibodies for 1 hour at RT. The following
695 primary antibodies used: anti-γ-H2AX (mouse, 1/200, Millipore, clone JBW301), anti-
696 TH (chicken, 1/500, Abcam, ab76442), anti-ORF1p (guinea pig, 1/200, in-house,
697 clone 09 as in [83], anti-mCherry (mouse, 1/200, Clontech 632543), rabbit anti-
698 H3K9me3 (rabbit, 1/200, Abcam, ab8898) and anti-MeCP2 (rabbit, 1/200, Millipore
699 MABE328). Sections were incubated with appropriate secondary antibodies (488
700 anti-chicken, 546 anti-mouse, 647 anti-guinea pig, 647 anti-rabbit, 647 anti-mouse,
701 Alexa Fluor, Life Technologies)
702
703 *In situ hybridization*
704 Mice were perfused with PBS in RNase-free conditions, and frozen in isopentane
705 (embedded in TissueTek O.C.T). Brain slices (20 µm) were fixed in 4% PFA in PBS
706 for 10 min at RT and then permeabilized twice for 10 min in RIPA buffer (150 mM
707 NaCl, 1% NP-40, 0.5% Na deoxycholate, 0.1% SDS, 1 mM EDTA, 50 mM Tris– HCl
708 pH 8). Brain sections were fixed again for 5 min in 4% PFA, acetylated for 10 min in
709 0.25% acetic anhydride (in 0. 1 M triethanolamine, pH 8). Sections were then
710 permeabilized for 30 min in PBS with 1% Triton X-100, 10 min in 10mM citrate buffer
711 pH6 at a 100°C and then pre-incubated for 1 h at 70°C in hybridization buffer (50%
712 formamide, 5× SSC, 5× Denhardt (1% Ficoll, 1% SSC, 1% Tween-20), 500 µg/ml
713 Salmon sperm DNA, 250 µg/ml yeast tRNA). Sections were then hybridized overnight
714 at 70 °C with a digoxigenin (DIG)-labeled RNA probes (DIG RNA labeling kit, Roche
715 11277073910) for *Gadd45b* mRNA. Sections were washed with FAM/SSC (50%
716 formamide, 2× SSC, 0.1% Tween-20) twice 30 min at 37°C, then twice in 0.2× SCC
717 at 42°C, blocked in B1 buffer (100 mM maleic acid pH 7.5, 150 mM NaCl) with 10%
718 fetal bovine serum (FBS) for 1 h, and incubated overnight at 4°C in B1 buffer with
719 alkaline phosphatase-conjugated anti-DIG (1/2000; Roche 11633716001) . After
720 three washes in B1 buffer and one wash in B3 buffer (100 mM Tris–HCl pH 9, 50 mM
721 $MgCl_2$, 100 mM NaCl, 0.1% Tween-20) for 15 min, slides were stained using the
722 NBT/ BCIP kit (Vector labs, SK5400), stopped with ddH_20 and slides were mounted
723 with DAKO-mounting medium.
724
725 *Imaging/ Microscopy*

726 All large field images used for TH+ neuron quantification, level of viral infection
727 quantification and striatal intensity quantification were made on widefield microscope
728 (Axio zoom V16 – Zeiss – Apotome.2) at 2,3 magnification with a zoom factor of
729 100. ISH image was taken by upright widefield microscope equipped with a color
730 CCD camera (Nikon 90i microscope) at 20x magnification in brightfield. H3K9me3,
731 MeCP2 and γ-H2AX foci quantification as well as ORF1p intensity quantification were
732 made on images taken by spinning disk microscopy (Yokogawa W1 Spinnning-disk
733 head mounted on an inverted Zeiss AxioObserver Z1) at 63x magnification.
734 The images in the figures are for illustration purposes and were taken by
735 confocal microscopy (LSM 980 with Airyscan 2, Zeiss) at 63x magnification with a
736 zoom factor of 1.4, except for the MeCP2 and ORF1p images (performed on the
737 spinning-disk microscope).
738
739 *Cell counting and image quantification*
740 TH cell counting in conditions comparing ipsi- (treated) and contralateral (non-
741 treated) sides were done as follows: For every brain, a minimum of four serial
742 sections were stained, and the number of TH cells was counted in the SNpc of both
743 ipsi- and contralateral sides. An ipsi/contra ratio was calculated for each section, and
744 the resulting mean of four sections was used to quantify the difference between the
745 TH cell number of the ipsi- and contralateral side of the same animal. The counting
746 was done blindly.
747 The quantification of axonal degeneration in the striatum comparing ipsi- and
748 contralateral sides was done as follows: For every brain, a minimum of seven serial
749 sections were stained, and the integrated density of TH staining intensity was
750 measured in ImageJ by determining the entire contralateral striatum as region of
751 interest (ROI) and conserving area for the measurement of ipsilateral sides. An
752 ipsi/contra ratio was calculated for each section, and the mean ratio of sections
753 containing the striatum was used to quantify the difference between TH striatal
754 intensity of the ipsi- and contralateral side of the same animal. The quantification was
755 done blindly.
756 Quantifications of foci were performed using a 63× magnification and 0.3 µm -
757 thick successive focal planes except for γ-H2AX foci quantification, which was made
758 using 0.2 µm-thick successive focal planes. Immunostainings of one parameter
759 (H3K9, MeCP2, Etc.) were all done in one experiment for all the conditions. For each

760 immunostaining, 3 images of the SNpc per side were taken on 3 sections per mouse,
761 thus 18 images per mouse (n=3 per condition), or 54 images per condition. The same
762 parameters were set-up on the spinning disk microscope to allow for comparison
763 between experimental conditions for the same staining. Images were analyzed by the
764 same experimenter using ImageJ software [84]. For foci quantifications the foci
765 counting Fiji Plug-in was used [85]. In addition, an image analysis plug-in was
766 developed for the ImageJ/Fiji software, using Bio-Format (openmicroscopy.org),
767 mcib3D [86] and GDSC (Alex Herbert from Sussex University) libraries. First, nuclei
768 that belonged to TH+ neurons were manually marked with the plug-in Cell Counter,
769 an xml file for each image containing 3D nuclei coordinates was saved. Then,
770 nucleus channel was filtered with a median filter (radius = 4) and a Difference of
771 Gaussian (DOG) (sigma1 = 30, sigma2 = 15), a binary mask was done with an Otsu
772 threshold. Only nuclei that are associated to the nuclei defined in the xml file were
773 kept. MeCP2 and H3K9me3 foci detections were performed using a median filter
774 (radius=2), DOG (sigma1=10, sigma2=2), binary mask was done with a MaxEntropy
775 threshold, then 3D objects (foci) that had a volume comprised between 1.5 and 40
776 μm^3 and were inside TH+ nuclei or at a 2 μm distance to nucleus was associated to
777 nuclei. γ-H2AX foci detection was performed using a median filter (radius=2), DOG
778 (sigma1=7, sigma2=3), binary mask was done with a Moments threshold, then 3D
779 objects (foci) that had a volume comprised between 0.5 and 100 μm^3 were inside
780 TH+ nuclei or at a 2 μm distance to nucleus was associated to nuclei. For each
781 nucleus, foci number, average foci volume, average foci integrated intensity and
782 average nucleus integrated intensity was computed.
783
784 *Gene ontology analysis*
785 Gene ontology analysis (PANTHER version 15.0; [87]) was done using the PANTHER
786 overrepresentation test with the GO-Slim annotation data sets 'biological process',
787 'molecular function' and cellular component' and the '*mus musculus*' gene set as the
788 reference list. Fisher's exact test was used to compute statistical significance of
789 overrepresentation with the false discovery rate (FDR) set at $p < 0.05$. The first 15
790 categories, ordered by fold enrichment, are displayed along with the corresponding
791 FDR value.
792

793 *Statistics*

794 Unless otherwise stated, the graphs represent each replicate and the error bar the
795 SEM of the mean of replicates. Error bars, values of n and mean ± SEM are as
796 stated in the figure legends. Results were considered as statistically significant for P-
797 value <0.05; in some cases, the exact P-value is given. Normality test were
798 performed prior to the statistical test and unless stated otherwise, the nonparametric
799 Wilcoxon-Mann-Whitney test was applied. All statistical analysis was done with the
800 software Prism.

801 For the bioinformatic analysis of the RRBS, we formulated the null hypothesis
802 that there are no differences in methylation between the two groups. After the p-
803 values have been computed, Methylkit, an R package for DNA methylation analysis
804 and annotation, uses the sliding window model (SLIM) to correct P-values to q-values
805 for multiple comparison tests. Statistically significant DMCs and DMRs were
806 identified with a q-value cutoff <0.01 and a methylation difference higher than 25%.

807

808 ***Acknowledgements***

809 This work was supported by the Fondation de France (00086320 to J.F.) and the
810 Fondation du Collège de France (to J.F.). We thank all primary donors for their
811 financial contributions to this work. We thank the animal facility members for their
812 essential contributions. We gratefully acknowledge Julien Dumont and the Collège de
813 France Orion imaging facility (IMACHEM-IBiSA), member of the French National
814 Research Infrastructure France-BioImaging (ANR-10-INBS-04), which received
815 support from the program «Investissements d'Avenir» ANR-10-LABX-54 MEMOLIFE.
816 We thank Yves Dupraz for the manufacturing of a customized mouse brain slicer.

817

818 ***Author contributions***

819 *CRG performed most of the experiments and participated in the writing of the*
820 *manuscript, OMB contributed experimentally, PM designed the semi-automated*
821 *image analysis workflow, AP co-supervised the beginning of the study, RLJ co-*
822 *supervised the study and contributed to the writing of the manuscript, JF co-*
823 *supervised the study, analyzed the RRBS data, wrote the manuscript and received*
824 *the funding.*

825 ***Figure Legends***

826

827 ***Figure1. Gadd45b overexpression in the SNpc of wildtype mice leads to***
828 ***perturbed DNA methylation.***

829 ***A****: Overview of the viral injection protocol into the SNpc of wild-type mice. Wild-type*
830 *OF1 mice were injected unilaterally in the SNpc with AAV8 virus expressing either*
831 *mCherry or mouse Gadd45b with its regulatory sequences under the control of the*
832 *Ef1a promoter. Animals were then sacrificed 14 or 90 days later to perform RRBS,*
833 *immunostainings or RT-qPCRs.*

834 ***B****: The AAV8-mCherry virus diffuses within the SNpc and infects mDA neurons.*
835 ***Upper panel****: TH and mCherry immunostaining of the SNpc of AAV8-mCherry*
836 *injected mice showing the diffusion of the virus in the SNpc area while sparing the*
837 *VTA. Scale bar represents 300 μm.* ***Lower pane****l: ISH of Gadd45b expression.*
838 *Gadd45b expression in the SNpc of AAV8-mGadd45b injected mice at 14d p.i.*
839 *shows that Gadd45b is overexpressed only in the ipsilateral SNpc and not in the*
840 *ipsilateral VTA, nor on the contralateral side.*

841 ***C:*** *Exogenous Gadd45b RNA is expressed 14d after the injection of AAV8-*
842 *mGadd45b. Transcript expression analysis by RT-qPCR following manual*
843 *microdissection of the SNpc of the injected side (****upper panel****) show a 79-fold*
844 *increase in mGadd45B transcript level (mCherry= 11.02±4.83; mGadd45B=*
845 *869.10±282.80 ; mean ± SEM) at 14d p.i. (left); n=6; and a 178 fold increase*
846 *(7.89±1.52; 1402±683) at 90d p.i. (right); n=4; *p<0,05; error bars represent SEM.*

847 ***D-I****: RRBS analysis of differentially methylated CpGs (DMCs) in the SNpc region*
848 *after injection of AAV8-mGadd45b or AAV8-control.*

849 ***D****: Volcano plot of differentially methylated CpGs shows widespread perturbations in*
850 *DNA methylation upon Gadd45b overexpression 14d p.i.. 76 185 significantly*
851 *differentially methylated CpGs were detected with a q-value smaller than or equal to*
852 *0.01 and at least 25% difference. The Volcano plot shows the number of regions with*
853 *changed patterns of methylation between Gadd45b and control samples significantly*
854 *higher or lower than the 25% difference cut-off and considering a q-value threshold of*
855 *0.01. The difference in methylation is reflected in the x-axis while the y-axis*
856 *represents the significance of the difference. Regions that are highly differentially*
857 *methylated are further to the left and right sides of the plot, while highly significant*
858 *changes appear higher on the plot. Values on the x- and y-axes are percent*

859 *methylation differences and negative log10 of the corrected p-values, respectively.*
860 *The pie chart shows the percentage of hyper- and hypomethylated regions.*
861 ***E and F**: DMCs are located majorly in open sea regions and in introns of genes.*
862 *DMCs were annotated in relation to the distance to a CpG island (E), as well as*
863 *based on the genomic regions they are associated with (**F**). Their distributions are*
864 *plotted in a bar chart.*
865 ***G**: Comparison of total number, common genetic intervals (minimum overlap of 1 bp)*
866 *and percentage in common for DMCs and DMRs 14d and 90d p.i..*
867 ***H**: The "Gadd45b-DMC-regulon". Venn diagrams showing the overlap of genes*
868 *containing at least one intronic hypomethylated DMC at 14 and 90d (4188 genes, left*
869 *upper Venn diagram), overlap of genes containing at least one hypermethylated*
870 *DMC at 14d and 90d (3827 genes, right upper Venn diagram) and the overlap of both*
871 *groups (2353 genes, lower Venn diagram) representing the "Gadd45b-DMC-*
872 *regulon". Note that the "Gadd45b-DMR-regulon" encomprising 447 genes is*
873 *summarized in the **Suppl. Fig.1E**.*
874 ***I**: GO-analysis of the "Gadd45b-DMC-regulon" reveals neuron-related gene*
875 *categories enriched after Gadd45b overexpression 14d p.i.. Gene ontology analysis*
876 *(PANTHER version 15.0) and the PANTHER overrepresentation test with the GO-*
877 *Slim annotation data set 'biological process' identified significantly overrepresented*
878 *GO categories. The first fifteen significantly overrepresented GO categories with the*
879 *highest fold enrichment are displayed with the fold enrichment on the left y-axis*
880 *(black points) and the FDR value on the right y-axis (grey points).*
881
882 ***Figure 2. Gadd45b overexpression leads to heterochromatin destructuration in***
883 ***mDA neurons.***
884 ***A-E:** H3K9me3 heterochromatin staining is perturbed as early as 14d after the*
885 *injection of AAV8-mGadd4b. TH+ neurons in the SNpc of AAV8-mGadd45b injected*
886 *mice (**A**) display at 14d p.i. a 1.13-fold increase in the number (3.64±0.12; 4.10±0.12,*
887 *data represented as a frequency distribution histogramm in **B**) and a 1.24-fold*
888 *increase in the volume (4.78±0.15; 5.91±0.22 μm^3, **C**) of H3K9me3 foci. The diffuse*
889 *nucleoplasmic staining intensity ($2.37x10^7$±557961; $1.96x10^7$±441292) is decreased*
890 *by 1.21-fold (**D**) while the foci intensity ($1.32x10^6$±54236; $1.41x10^6$±64942) remains*
891 *unchanged (**E**).*

892 ***F-J:*** *H3K9me3 heterochromatin staining remains perturbed up until 90d after the*
893 *injection of AAV8-mGadd45b. A similar pattern as in* ***A-E*** *was observed at 90d p.i.*
894 *with a 1.18-fold increase in the number (4.07±0.17; 4.82±0.20, data represented as a*
895 *frequency distribution histogramm in* ***G****) and a 1.15-fold increase in the volume*
896 *(5.51±0.18; 6.35±0.24 $\mu m^{3,}$* ***H****) of H3K9me3 foci shown in (****F****). The diffuse*
897 *nucleoplasmic staining intensity ($5.66x10^7$±$5x10^6$; $1.97x10^7$±573406) is decreased by*
898 *2.87-fold while the foci intensity ($1.22x10^6$±56943; $1.26x10^6$±74064) remains*
899 *unchanged (****I****;* ***J****). Scale bar in* ***A*** *and* ***F*** *represents 5 μm. ** p<0.01; *** p<0.001; ****
900 *p<0.0001; n=3 mice; Between 510 and 534 neurons were quantified per condition at*
901 *14d p.i. and 428 neurons were quantified per condition at 90d p.i.. Error bars*
902 *represent SEM.*
903
904 ***Figure 3. Loss of TH+ neurons and their increased vulnerability upon Gadd45b***
905 ***overexpression.***
906 ***A-C****: Dopaminergic cell loss in the SNpc 90d following the injection of AAV8-*
907 *mGadd45b. The ratio of the number of TH+ neurons of the injected side on the non-*
908 *injected side is similar at 14d p.i. between AAV8-mCherry and AAV8-mGadd4b*
909 *injected mice and close to 1 (1.04±0.02; 0.97±0.04) (****B****). At 90d p.i. however, if the*
910 *ratio of AAV8-mCherry mice is still close to 1 (0.97±0.02), the ratio of AAV8-*
911 *mGadd45b mice (0.82±0.04) reflect a 18 % loss of TH+ neurons compared to the*
912 *non-injected side, shown in (****A****) and quantified in (****C****); scale bar represents 1000 μm;*
913 *n=5.*
914 ***D-F****: Dopaminergic neurons are sensitized to 6-OHDA upon Gadd45b*
915 *overexpression. At 14d p.i., AAV8-mCherry and AAV8-mGadd45b mice were injected*
916 *with 6-OHDA in the striatum, on the same side as the viral injection and analyzed 3*
917 *days after (****Fig. 1A****). TH staining of dopaminergic axons shows that axonal*
918 *degeneration in the striatum induced by 6-OHDA occurs in AAV8-mCherry mice*
919 *(0.71±0.04) but is 1.5-fold more pronounced in AAV8-mGadd45b mice (0.56±0.04)*
920 *shown in (****D****), quantified in (****E****). The number of TH+ neurons is unaffected*
921 *(0.96±0.04; 0.85±0.03) after the 3 day 6-OHDA treatment (****F****); n= 4-6; Scale bar*
922 *represents 1000 μm.*
923 ***G-J****: Gadd45b expression accentuates heterochromatin loss and MeCP2 foci*
924 *dispersion upon striatal 6-OHDA injection. TH+ neurons in the SNpc of AAV8-*

925 *mGadd45b mice injected with 6-OHDA at 14d p.i. display 3 days after the 6-OHDA*
926 *injection an increase* by 1.47-fold *in the number of H3K9me3 foci* (3.28±0.15;
927 4.82±0.16)*, shown in (**G**), quantified and represented as a frequency distribution*
928 *histogramm in (**H**) and by 1.16-fold in the number of MeCP2 foci* (2.97±0.12;
929 3.45±0.08)*,shown in (**I**), quantified and represented as a frequency distribution*
930 *histogramm in (**J**). Scale bar represents 5 μm; * p<0,05; ** p<0,01; **** p<0,0001;*
931 *n=3; Between 632 and 887 neurons were quantified per condition for H3K9me3 foci*
932 *and between 94 and 276 neurons per condition for MeCP2 foci. Error bars represent*
933 *SEM.*
934
935 ***Figure 4. DNA methylation changes and heterochromatin de-structuration upon***
936 ***Gadd45b overexpression are associated with DNA damage.***
937 ***A-C:*** *Gadd45b overexpression induced DNA damage in TH+ neurons of the SNpc.*
938 *The majority (65.94±2.10 %) of TH+ neurons of the SNpc in AAV8-mGadd45b*
939 *display no single* γ-H2AX *foci but instead an intense diffuse nucleoplasmic staining,*
940 *1.7-times more than in AAV8-mCherry mice (39.81±2.40 %), shown in (**A**), number*
941 *quantified in (**B**), diffuse nucleoplasmic intensity quantified and represented as a*
942 *frequency distribution histogram in (**C**). Scale bar represents 5 μm; n=3. Between*
943 *417 and 518 neurons were quantified per condition.*
944
945 ***Figure 5. LINE-1 methylation changes and increased LINE-1 expression***
946 ***following Gadd45b overexpression.***
947 ***A-C:*** *Analysis of DMCs in LINE-1 sequences (L1-DMCs) 14d p.i. of AAV8-*
948 *mGadd45b.*
949 ***A****: Location of L1-DMCs. 22.5% of all (3530 L1-DMCs are located in introns.*
950 ***B****: Of all the L1-DMCs at 14d p.i., most (54.7%) are hypomethylated (blue).*
951 ***C****: The ten most represented L1 families with at least one L1-DMC.*
952 ***D-G:*** *Analysis of DMCs in intronic LINE-1 sequences (L1-iDMCs) 14d p.i. of AAV8-*
953 *mGadd45b.*
954 *Most L1-iDMCs (54.7%) are hypomethylated (**D**), located in protein-coding genes (in*
955 *483 genes, **E**) and related to neuronal functions (**F**).*
956 ***G****: The ten most represented L1 families with L1-iDMCs.*

957 ***H**: Analysis of the methylation status of full-length LINE-1 (flL1) elements containing*
958 *a DMC or a DMR. Most DMCs and DMRs in full-length L1 elements are*
959 *hypomethylated.*
960 ***I:** LINE-1 transcripts of the young L1Md-T and L1Md-A families are increased after*
961 *injection of AAV8-mGadd45b compared to AAV8-mCherry 14d p.i.. RT-qPCR of RNA*
962 *extracted from manually micro-dissected SNpc of the injected sides shows a 1.5-fold*
963 *increase in L1 A transcripts level (**left**) (512.40±38.48; 782.60±87.44) and 1.4-fold*
964 *increase in L1 Tf/Gf transcripts level (**right**) (190.80±13.63; 261.20±28.28) in AAV8-*
965 *mGadd45B mice at 14d p.i. compared to AAV8-mCherry mice; * p<0,05; ** p<0,01;*
966 ***** p<0,0001; n=6. Error bars represent SEM.*
967
968 ***Figure 6: Candidate genes with DMCs upon Gadd45b overexpression show***
969 ***altered expression in the SNpc at 90d p.i.***
970 ***A:** The expression of several gene candidates containing DMCs is dysregulated.*
971 *Setdb1, Park2 Dnmt3a, Tet3 and Satb1 transcripts are downregulated 90d p.i. of*
972 *AAV8-mGadd45b. The mRNA analysis in SNpc of the injected side by RT-qPCR*
973 *shows no significant difference in Satb1 (4.87±0.59; 5.57±0.65), Setdb1 (9.03±0.76;*
974 *7.51±0.42), Dnmt3a (24.07±2.52; 22.76±0.92), Tet3 (2.16±0.26; 2.20±0.65) and*
975 *Park2 (1.46±0.21; 1.65±0.09) transcripts at 14d p.i. (4.87±0.59; 5.57±0.65); n=5-6. At*
976 *90d p.i., there is a decrease in transcript levels of 1.9-fold for Satb1 (4.43±0.30;*
977 *2.31±0.62), of 1.15-fold for Setdb1 (12.32±0.20; 10.68±0.34) of 1.11-fold for Dnmt3a*
978 *(30.06±0.47; 27.05±0.67), of 1.14 fold for Tet3 (3.89±0.09; 3.40±0.17) of 1.25-fold*
979 *for Park2 (3.42±0.12; 2.73±0.18), in AAV8-mGadd45b mice compared to AAV8-*
980 *mCherry mice; * p<0,05; n=4. Error bars represent SEM.*
981 ***B:** Genes significantly deregulated upon Gadd45b overexpression were analyzed*
982 *with regard to methylation differences throughout their gene bodies (exonic and*
983 *intronic DMCs) at 14d and 90d p.i.. Results are displayed for Satb1, Setdb1, Dnmt3a,*
984 *Tet3 and Park2. Exact chromosomal positions of DMCs are given on the x-axis and*
985 *the orientation of the genes is indicated by an arrow. Hypermethylated are depicted*
986 *as red squares while hypomethylated DMCs are depicted in blue squares. DMCs*
987 *were defined as having a methylation difference > or equal to 25 (dashed line) and a*
988 *q-value <0.01.*
989

990 ***Table 1. Summary of the differential methylation analysis comparing Gadd45b***
991 ***overexpression to mCherry control in the SNpc of wild-type mice.***

992 **References**

993

994 1. Solovei, I., Thanisch, K. & Feodorova, Y. How to rule the nucleus: divide et
995 impera. *Curr. Opin. Cell Biol.* 40, 47–59 (2016).
996 2. Benayoun, B. A., Pollina, E. A. & Brunet, A. Epigenetic regulation of ageing:
997 linking environmental inputs to genomic stability. *Nat. Rev. Mol. Cell Biol.* 16,
998 593–610 (2015).
999 3. Pal, S. & Tyler, J. K. Epigenetics and aging. *Sci. Adv.* 2, e1600584–19 (2016).
1000 4. Lodato, M. A. *et al.* Aging and neurodegeneration are associated with
1001 increased mutations in single human neurons. *Science* (2017).
1002 doi:10.1126/science.aao4426
1003 5. Burgess, R. C., Misteli, T. & Oberdoerffer, P. DNA damage, chromatin, and
1004 transcription: the trinity of aging. *Curr. Opin. Cell Biol.* 24, 724–730 (2012).
1005 6. Lander, E. S. *et al.* Initial sequencing and analysis of the human genome.
1006 *Nature* 409, 860–921 (2001).
1007 7. Mouse Genome Sequencing Consortium *et al.* Initial sequencing and
1008 comparative analysis of the mouse genome. *Nature* 420, 520–562 (2002).
1009 8. Trelogan, S. A. & Martin, S. L. Tightly regulated, developmentally specific
1010 expression of the first open reading frame from LINE-1 during mouse
1011 embryogenesis. *Proc. Natl. Acad. Sci. U.S.A.* 92, 1520–1524 (1995).
1012 9. Wei, W. *et al.* Human L1 retrotransposition: cis preference versus trans
1013 complementation. *Molecular and Cellular Biology* 21, 1429–1439 (2001).
1014 10. Martin, S. L. & Bushman, F. D. Nucleic acid chaperone activity of the ORF1
1015 protein from the mouse LINE-1 retrotransposon. *Molecular and Cellular Biology*
1016 21, 467–475 (2001).
1017 11. Hattori, M., Kuhara, S., Takenaka, O. & Sakaki, Y. L1 family of repetitive DNA
1018 sequences in primates may be derived from a sequence encoding a reverse
1019 transcriptase-related protein. *Nature* 321, 625–628 (1986).
1020 12. Feng, Q., Moran, J. V., Kazazian, H. H. & Boeke, J. D. Human L1
1021 retrotransposon encodes a conserved endonuclease required for
1022 retrotransposition. *Cell* 87, 905–916 (1996).
1023 13. Pizarro, J. G. & Cristofari, G. Post-Transcriptional Control of LINE-1
1024 Retrotransposition by Cellular Host Factors in Somatic Cells. *Front Cell Dev*
1025 *Biol* 4, 14 (2016).
1026 14. Van Meter, M. *et al.* SIRT6 represses LINE1 retrotransposons by ribosylating
1027 KAP1 but this repression fails with stress and age. *Nat Commun* 5, 5011
1028 (2014).
1029 15. Kazazian, H. H. & Goodier, J. L. LINE drive. retrotransposition and genome
1030 instability. *Cell* 110, 277–280 (2002).
1031 16. Gasior, S. L., Wakeman, T. P., Xu, B. & Deininger, P. L. The human LINE-1
1032 retrotransposon creates DNA double-strand breaks. *J. Mol. Biol.* 357, 1383–
1033 1393 (2006).
1034 17. Simon, M. *et al.* LINE1 Derepression in Aged Wild-Type and SIRT6- Deficient
1035 Mice Drives Inflammation. *Cell Metab.* 1–21 (2019).
1036 doi:10.1016/j.cmet.2019.02.014
1037 18. Blaudin de Thé, F.-X. *et al.* Engrailed homeoprotein blocks degeneration in
1038 adult dopaminergic neurons through LINE-1 repression. *EMBO J* 37, (2018).

1039 19. Collier, T. J., Kanaan, N. M. & Kordower, J. H. Ageing as a primary risk factor
1040 for Parkinson's disease: evidence from studies of non-human primates. *Nat*
1041 *Rev Neurosci* 12, 359–366 (2011).
1042 20. López-Otín, C., Blasco, M. A., Partridge, L., Serrano, M. & Kroemer, G. The
1043 hallmarks of aging. *Cell* 153, 1194–1217 (2013).
1044 21. Gan, L., Cookson, M. R., Petrucelli, L. & La Spada, A. R. Converging pathways
1045 in neurodegeneration, from genetics to mechanisms. *Nat Neurosci* 21, 1300–
1046 1309 (2018).
1047 22. Hou, Y. *et al.* Ageing as a risk factor for neurodegenerative disease. *Nat Rev*
1048 *Neurol* 15, 565–581 (2019).
1049 23. Fasolino, M., Liu, S., Wang, Y. & Zhou, Z. Distinct cellular and molecular
1050 environments support aging-related DNA methylation changes in the
1051 substantia nigra. *Epigenomics* 9, 21–31 (2017).
1052 24. Sanchez-Mut, J. V. *et al.* Human DNA methylomes of neurodegenerative
1053 diseases show common epigenomic patterns. 6, e718–8 (2016).
1054 25. Labbé, C., Lorenzo-Betancor, O. & Ross, O. A. Epigenetic regulation in
1055 Parkinson's disease. *Acta Neuropathol* 132, 515–530 (2016).
1056 26. Park, G. *et al.* Regulation of Histone Acetylation by Autophagy in Parkinson
1057 Disease. *Journal of Biological Chemistry* 291, 3531–3540 (2016).
1058 27. Gavin, D. P. *et al.* Gadd45b and N-methyl-D-aspartate induced DNA
1059 demethylation in postmitotic neurons. *Epigenomics* 7, 567–579 (2015).
1060 28. Niehrs, C. & Schäfer, A. Active DNA demethylation by Gadd45 and DNA
1061 repair. *Trends Cell Biol.* 22, 220–227 (2012).
1062 29. Ma, D. K. *et al.* Neuronal Activity-Induced Gadd45b Promotes Epigenetic DNA
1063 Demethylation and Adult Neurogenesis. *Science* 323, 1074–1077 (2009).
1064 30. Rekaik, H. *et al.* Engrailed Homeoprotein Protects Mesencephalic
1065 Dopaminergic Neurons from Oxidative Stress. *CellReports* 13, 242–250
1066 (2015).
1067 31. Chen, K. *et al.* Gadd45a is a heterochromatin relaxer that enhances iPS cell
1068 generation. *EMBO reports* 17, 1641–1656 (2016).
1069 32. Blandini, F., Armentero, M.-T. & Martignoni, E. The 6-hydroxydopamine model:
1070 news from the past. *Parkinsonism and realted Disorders* 14 Suppl 2, S124–9
1071 (2008).
1072 33. Bagga, V., Dunnett, S. B. & Fricker, R. A. The 6-OHDA mouse model of
1073 Parkinson's disease - Terminal striatal lesions provide a superior measure of
1074 neuronal loss and replacement than median forebrain bundle lesions. *Behav.*
1075 *Brain Res.* 288, 107–117 (2015).
1076 34. Villeponteau, B. The heterochromatin loss model of aging. *Exp. Gerontol.* 32,
1077 383–394 (1997).
1078 35. Peters, A. H. *et al.* Loss of the Suv39h histone methyltransferases impairs
1079 mammalian heterochromatin and genome stability. *Cell* 107, 323–337 (2001).
1080 36. Pegoraro, G. *et al.* Ageing-related chromatin defects through loss of the NURD
1081 complex. *Nature Cell Biology* 11, 1261–1267 (2009).
1082 37. Sun, W., Samimi, H., Gamez, M., Zare, H. & Frost, B. Pathogenic tau-induced
1083 piRNA depletion promotes neuronal death through transposable element
1084 dysregulation in neurodegenerative tauopathies. *Nat Neurosci* 21, 1038–1048
1085 (2018).
1086 38. Frost, B., Hemberg, M., Lewis, J. & Feany, M. B. Tau promotes
1087 neurodegeneration through global chromatin relaxation. *Nat Neurosci* 17, 357–
1088 366 (2014).

1089 39. Hajjar, El, J. *et al.* Heterochromatic genome instability and neurodegeneration
1090 sharing similarities with Alzheimer's disease in old Bmi1+/- mice. *Sci. Rep.* 1–
1091 16 (2019). doi:10.1038/s41598-018-37444-3
1092 40. Belgnaoui, S. M., Gosden, R. G., Semmes, O. J. & Haoudi, A. Human LINE-1
1093 retrotransposon induces DNA damage and apoptosis in cancer cells. *Cancer*
1094 *Cell Int.* 6, 13 (2006).
1095 41. Sookdeo, A., Hepp, C. M., McClure, M. A. & Boissinot, S. Revisiting the
1096 evolution of mouse LINE-1 in the genomic era. *Mob DNA* 4, 1–1 (2013).
1097 42. Penzkofer, T. *et al.* L1Base 2: more retrotransposition-active LINE-1s, more
1098 mammalian genomes. *Nucleic Acids Research* 45, D68–D73 (2017).
1099 43. Blaudin de Thé, F.-X., Rekaik, H., Prochiantz, A., Fuchs, J. & Joshi, R. L.
1100 Neuroprotective Transcription Factors in Animal Models of Parkinson Disease.
1101 *Neural Plast.* 2016, 6097107 (2016).
1102 44. Li, Z. *et al.* Gadd45a promotes DNA demethylation through TDG. *Nucleic Acids*
1103 *Research* 43, 3986–3997 (2015).
1104 45. Labonté, B. *et al.* Gadd45b mediates depressive-like role through DNA
1105 demethylation. *Sci. Rep.* 9, 4615 (2019).
1106 46. Gavin, D. P. *et al.* Growth arrest and DNA-damage-inducible, beta (GADD45b)-
1107 mediated DNA demethylation in major psychosis. *Neuropsychopharmacology*
1108 37, 531–542 (2012).
1109 47. Apulei, J. *et al.* Non-cell Autonomous OTX2 Homeoprotein Regulates Visual
1110 Cortex Plasticity Through Gadd45b/g. *Cereb. Cortex* 29, 2384–2395 (2019).
1111 48. Kienhöfer, S. *et al.* GADD45a physically and functionally interacts with TET1.
1112 *Differentiation* 90, 59–68 (2015).
1113 49. Arab, K. *et al.* GADD45A binds R-loops and recruits TET1 to CpG island
1114 promoters. *Nat Genet* 1–13 (2018). doi:10.1038/s41588-018-0306-6
1115 50. Bayraktar, G. & Kreutz, M. R. The Role of Activity-Dependent DNA
1116 Demethylation in the Adult Brain and in Neurological Disorders. *Front Mol*
1117 *Neurosci* 11, 169 (2018).
1118 51. Lee, M. *et al.* Epigenomic analysis of Parkinson's disease neurons identifies
1119 Tet2 loss as neuroprotective. *bioRxiv* 779785 (2019).
1120 52. Perera, A. *et al.* TET3 Is Recruited by REST for Context-Specific
1121 Hydroxymethylation and Induction of Gene Expression. *CellReports* 11, 283–
1122 294 (2015).
1123 53. Jin, S.-G. *et al.* Tet3 Reads 5-Carboxylcytosine through Its CXXC Domain and
1124 Is a Potential Guardian against Neurodegeneration. *CellReports* 14, 493–505
1125 (2016).
1126 54. Chuang, Y.-H. *et al.* Longitudinal Epigenome-Wide Methylation Study of
1127 Cognitive Decline and Motor Progression in Parkinson's Disease. *J Parkinsons*
1128 *Dis* 9, 389–400 (2019).
1129 55. Pihlstrøm, L., Berge, V., Rengmark, A. & Toft, M. Parkinson's disease
1130 correlates with promoter methylation in the α-synuclein gene. *Mov Disord.* 30,
1131 577–580 (2015).
1132 56. Wüllner, U., Kaut, O., deBoni, L., Piston, D. & Schmitt, I. DNA methylation in
1133 Parkinson's disease. *J Neurochem* 139 Suppl 1, 108–120 (2016).
1134 57. Li, P. *et al.* Epigenetic dysregulation of enhancers in neurons is associated with
1135 Alzheimerâ€™s disease pathology and cognitive symptoms. *Nat Commun* 1–
1136 14 (2019). doi:10.1038/s41467-019-10101-7
1137 58. Nativio, R. *et al.* Dysregulation of the epigenetic landscape of normal aging in
1138 Alzheimer's disease. *Nat Neurosci* 21, 497–505 (2018).

1139 59. Berson, A., Nativio, R., Berger, S. L. & Bonini, N. M. Epigenetic Regulation in
1140 Neurodegenerative Diseases. *Trends in Neurosciences* 41, 587–598 (2018).
1141 60. Cedar, H. & Bergman, Y. Linking DNA methylation and histone modification:
1142 patterns and paradigms. *Nature Reviews Genetics* 10, 295–304 (2009).
1143 61. Schäfer, A. Gadd45 proteins: key players of repair-mediated DNA
1144 demethylation. *Adv. Exp. Med. Biol.* 793, 35–50 (2013).
1145 62. Suberbielle, E. *et al.* Physiologic brain activity causes DNA double-strand
1146 breaks in neurons, with exacerbation by amyloid-β. *Nature Publishing Group*
1147 (2013). doi:10.1038/nn.3356
1148 63. Simon, M. *et al.* Inhibition of retrotransposition improves health and extends
1149 lifespan of SIRT6 knockout mice. 1–53 (2018). doi:10.1101/460808
1150 64. De Cecco, M. *et al.* Transposable elements become active and mobile in the
1151 genomes of aging mammalian somatic tissues. *Aging (Albany NY)* 5, 867–883
1152 (2013).
1153 65. Li, W. *et al.* Activation of transposable elements during aging and neuronal
1154 decline in Drosophila. *Nature Publishing Group* (2013). doi:10.1038/nn.3368
1155 66. Wood, J. G. *et al.* Chromatin-modifying genetic interventions suppress age-
1156 associated transposable element activation and extend life span in Drosophila.
1157 *Proceedings of the National Academy of Sciences* 201604621 (2016).
1158 doi:10.1073/pnas.1604621113
1159 67. Liu, E. Y. *et al.* Loss of Nuclear TDP-43 Is Associated with Decondensation of
1160 LINE Retrotransposons. *CellReports* 27, 1409–1421.e6 (2019).
1161 68. Billingsley, K. J. *et al.* Analysis of repetitive element expression in the blood
1162 and skin of patients with Parkinson's disease identifies differential expression
1163 of satellite elements. *Sci. Rep.* 9, 4369 (2019).
1164 69. Li, W., Jin, Y., Prazak, L., Hammell, M. & Dubnau, J. Transposable elements in
1165 TDP-43-mediated neurodegenerative disorders. *PLoS ONE* 7, e44099 (2012).
1166 70. Södersten, E. *et al.* A comprehensive map coupling histonemodifications with
1167 gene regulation in adultdopaminergic and serotonergic neurons. *Nat Commun*
1168 1–16 (2018). doi:10.1038/s41467-018-03538-9
1169 71. Zahn, J. M. *et al.* AGEMAP: a gene expression database for aging in mice.
1170 *PLoS Genet* 3, e201 (2007).
1171 72. Urdinguio, R. G., Sanchez-Mut, J. V. & Esteller, M. Epigenetic mechanisms in
1172 neurological diseases: genes, syndromes, and therapies. *Lancet Neurol* 8,
1173 1056–1072 (2009).
1174 73. Hodges, A. *et al.* Regional and cellular gene expression changes in human
1175 Huntington's disease brain. *Human Molecular Genetics* 15, 965–977 (2006).
1176 74. Narayanan, M. *et al.* Common dysregulation network in the human prefrontal
1177 cortex underlies two neurodegenerative diseases. *Mol. Syst. Biol.* 10, 743–743
1178 (2014).
1179 75. Prudencio, M. *et al.* Distinct brain transcriptome profiles in C9orf72-associated
1180 and sporadic ALS. *Nat Neurosci* 18, 1175–1182 (2015).
1181 76. Soukup, S.-F. & Verstreken, P. PIWIL1 protein power targets tau therapy. *Nat*
1182 *Neurosci* 17, 334–335 (2014).
1183 77. Soukup, S.-F., Vanhauwaert, R. & Verstreken, P. Parkinson's disease:
1184 convergence on synaptic homeostasis. *EMBO J* (2018).
1185 doi:10.15252/embj.201898960
1186 78. Burke, R. E. & O'Malley, K. Axon degeneration in Parkinson's disease.
1187 *Experimental Neurology* 246, 72–83 (2013).

1188 79. Jones, P. A. Functions of DNA methylation: islands, start sites, gene bodies
1189 and beyond. *Nature Reviews Genetics* 13, 484–492 (2012).
1190 80. Kinde, B., Gabel, H. W., Gilbert, C. S., Griffith, E. C. & Greenberg, M. E.
1191 Reading the unique DNA methylation landscape of the brain: Non-CpG
1192 methylation, hydroxymethylation, and MeCP2. *Proceedings of the National*
1193 *Academy of Sciences* 112, 201411269 (2015).
1194 81. Neri, F. *et al.* Intragenic DNA methylation prevents spurious transcription
1195 initiation. *Nature* 1–30 (2017). doi:10.1038/nature21373
1196 82. Yang, X. *et al.* Gene body methylation can alter gene expression and is a
1197 therapeutic target in cancer. *Cancer Cell* 26, 577–590 (2014).
1198 83. Cancio-Bello, A. & Saez-Atienzar, S. SATB1 is a dopaminergic neuron-specific
1199 regulator of cellular senescence. *Mov Disord.* 35, 235–235 (2020).
1200 84. Riessland, M. *et al.* Loss of SATB1 Induces p21-Dependent Cellular
1201 Senescence in Post-mitotic Dopaminergic Neurons. *Cell Stem Cell* 25, 514–
1202 530.e8 (2019).
1203 85. Yasui, D., Miyano, M., Cai, S., Varga-Weisz, P. & Kohwi-Shigematsu, T.
1204 SATB1 targets chromatin remodelling to regulate genes over long distances.
1205 *Nature* 419, 641–645 (2002).
1206 86. Cai, S., Han, H.-J. & Kohwi-Shigematsu, T. Tissue-specific nuclear architecture
1207 and gene expression regulated by SATB1. *Nat Genet* 34, 42–51 (2003).
1208 87. Zhang, X. *et al.* DNMT3A and TET2 compete and cooperate to repress
1209 lineage-specific transcription factors in hematopoietic stem cells. *Nat Genet* 48,
1210 1014–1023 (2016).
1211 88. Krueger, F. & Andrews, S. R. Bismark: a flexible aligner and methylation caller
1212 for Bisulfite-Seq applications. *Bioinformatics* 27, 1571–1572 (2011).
1213 89. Akalin, A. *et al.* methylKit: a comprehensive R package for the analysis of
1214 genome-wide DNA methylation profiles. *Genome Biol* 13, R87 (2012).
1215 90. Cavalcante, R. G. & Sartor, M. A. annotatr: genomic regions in context.
1216 *Bioinformatics* 33, 2381–2383 (2017).

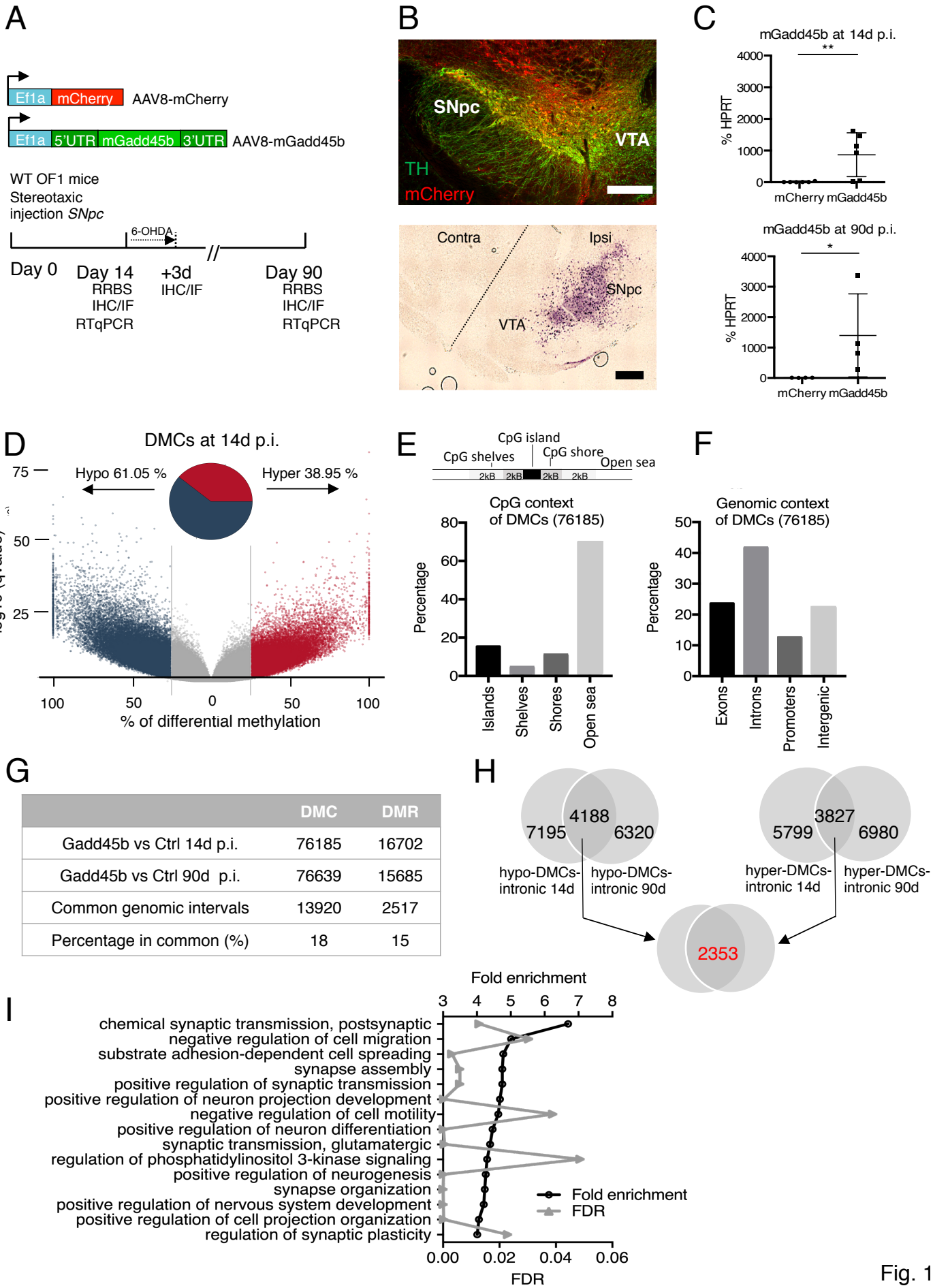

	DMC	DMR
Gadd45b vs Ctrl 14d p.i.	76185	16702
Gadd45b vs Ctrl 90d p.i.	76639	15685
Common genomic intervals	13920	2517
Percentage in common (%)	18	15

Fig. 1

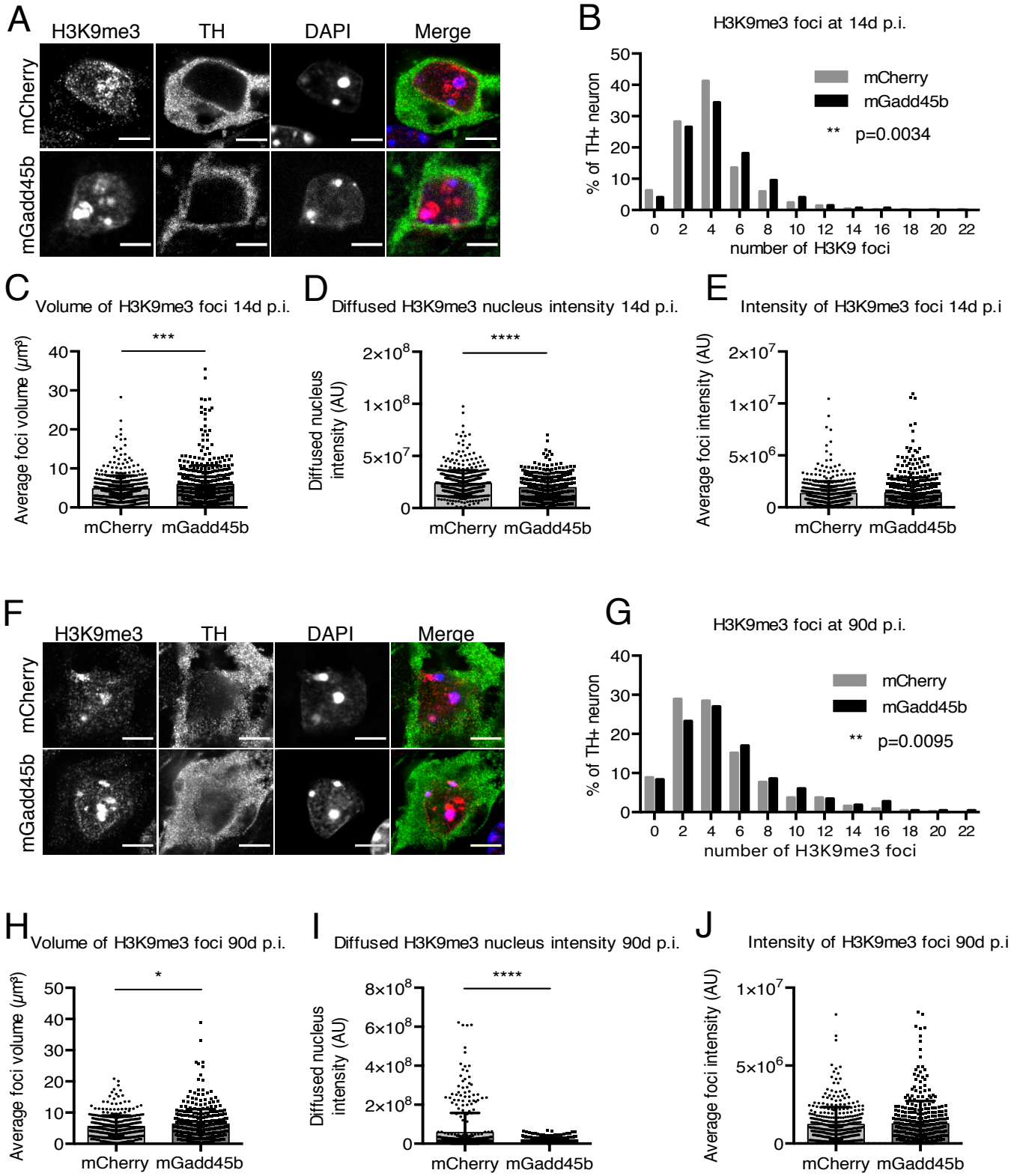
A
H3K9me3
TH
DAPI
Merge
mCherry
mGadd45b
B
H3K9me3 foci at 14d p.i.
% of TH+ neuron
mCherry
mGadd45b
** p=0.0034
number of H3K9 foci
C
Volume of H3K9me3 foci 14d p.i.
Average foci volume (μm³)
***
mCherry
mGadd45b
D
Diffused H3K9me3 nucleus intensity 14d p.i.
Diffused nucleus intensity (AU)
****
E
Intensity of H3K9me3 foci 14d p.i
Average foci intensity (AU)
F
G
H3K9me3 foci at 90d p.i.
** p=0.0095
number of H3K9me3 foci
H
Volume of H3K9me3 foci 90d p.i.
*
I
Diffused H3K9me3 nucleus intensity 90d p.i.
J
Intensity of H3K9me3 foci 90d p.i

Fig. 2

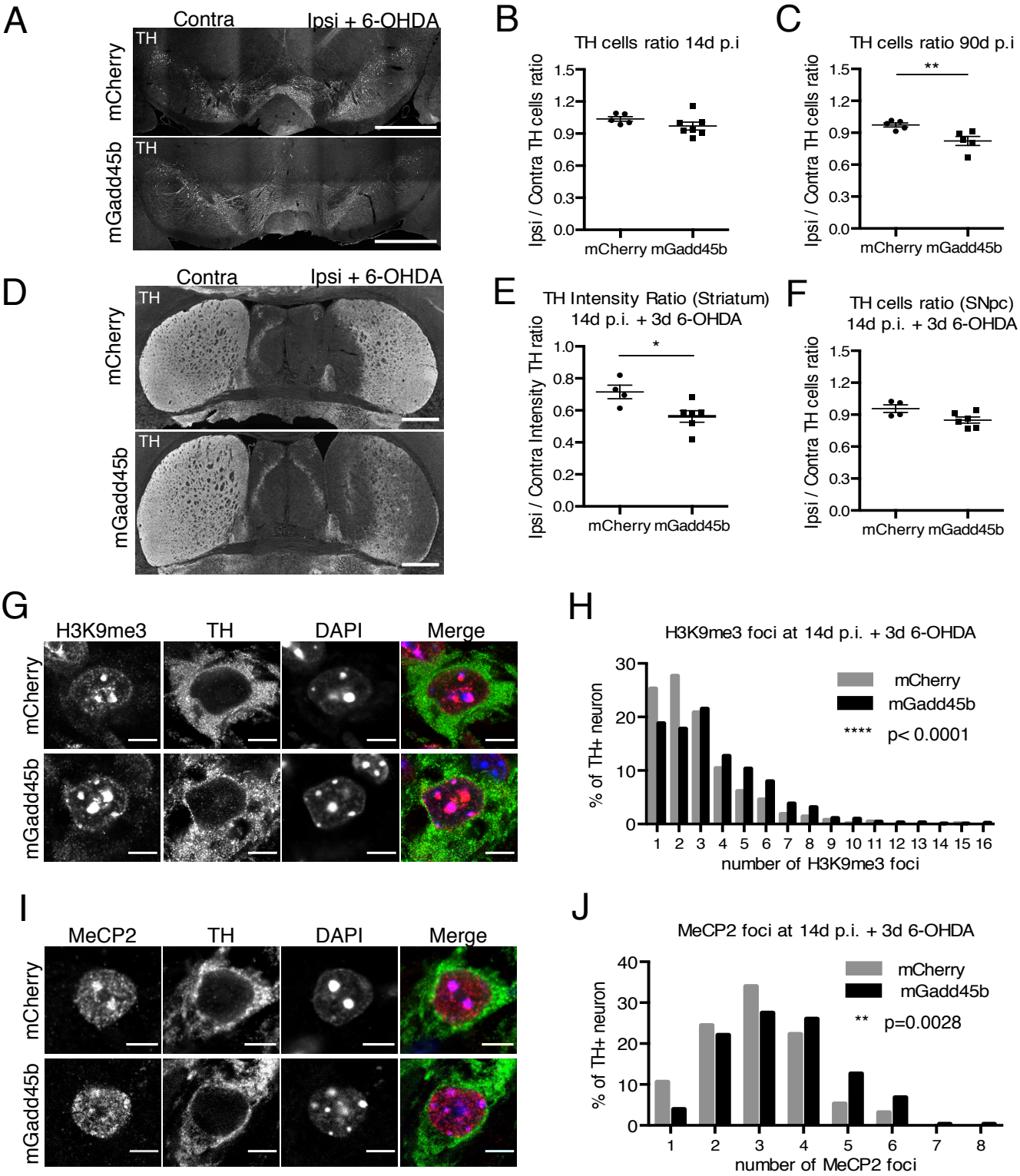
A
Contra
Ipsi + 6-OHDA
mCherry
mGadd45b
TH
B
TH cells ratio 14d p.i
Ipsi / Contra TH cells ratio
mCherry mGadd45b
C
TH cells ratio 90d p.i
**
D
E
TH Intensity Ratio (Striatum)
14d p.i. + 3d 6-OHDA
Ipsi / Contra Intensity TH ratio
*
F
TH cells ratio (SNpc)
14d p.i. + 3d 6-OHDA
G
H3K9me3
TH
DAPI
Merge
H
H3K9me3 foci at 14d p.i. + 3d 6-OHDA
% of TH+ neuron
mCherry
mGadd45b
**** p< 0.0001
number of H3K9me3 foci
I
MeCP2
J
MeCP2 foci at 14d p.i. + 3d 6-OHDA
** p=0.0028
number of MeCP2 foci

Fig. 3

A

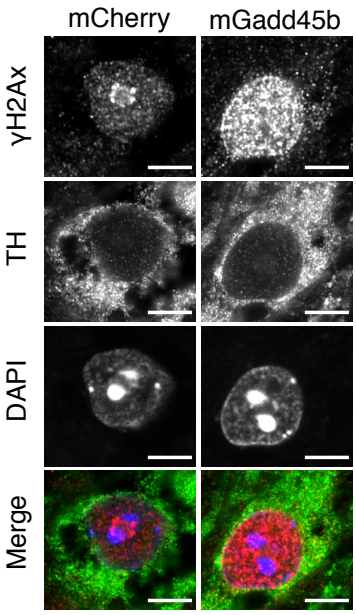
mCherry
mGadd45b
γH2Ax
TH
DAPI
Merge

B

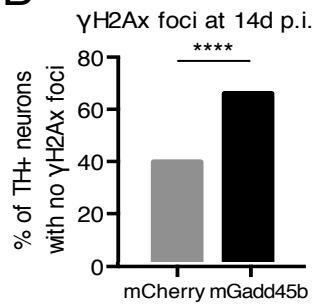
γH2Ax foci at 14d p.i.
****
% of TH+ neurons with no γH2Ax foci
80
60
40
20
0
mCherry
mGadd45b

C

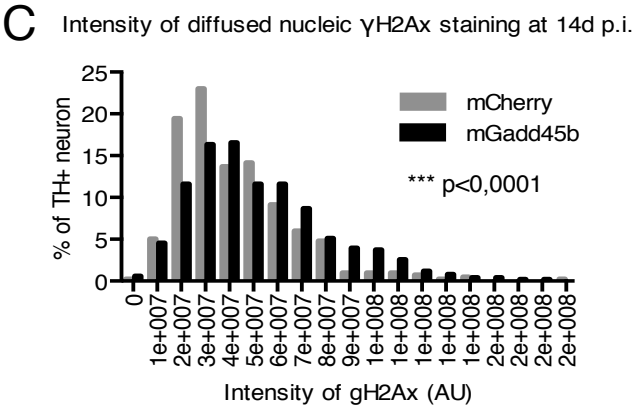
Intensity of diffused nucleic γH2Ax staining at 14d p.i.
% of TH+ neuron
25
20
15
10
5
0
mCherry
mGadd45b
*** p<0,0001
0
1e+007
2e+007
3e+007
4e+007
5e+007
6e+007
7e+007
8e+007
9e+007
1e+008
1e+008
1e+008
1e+008
1e+008
2e+008
2e+008
2e+008
2e+008
Intensity of gH2Ax (AU)

Fig. 4

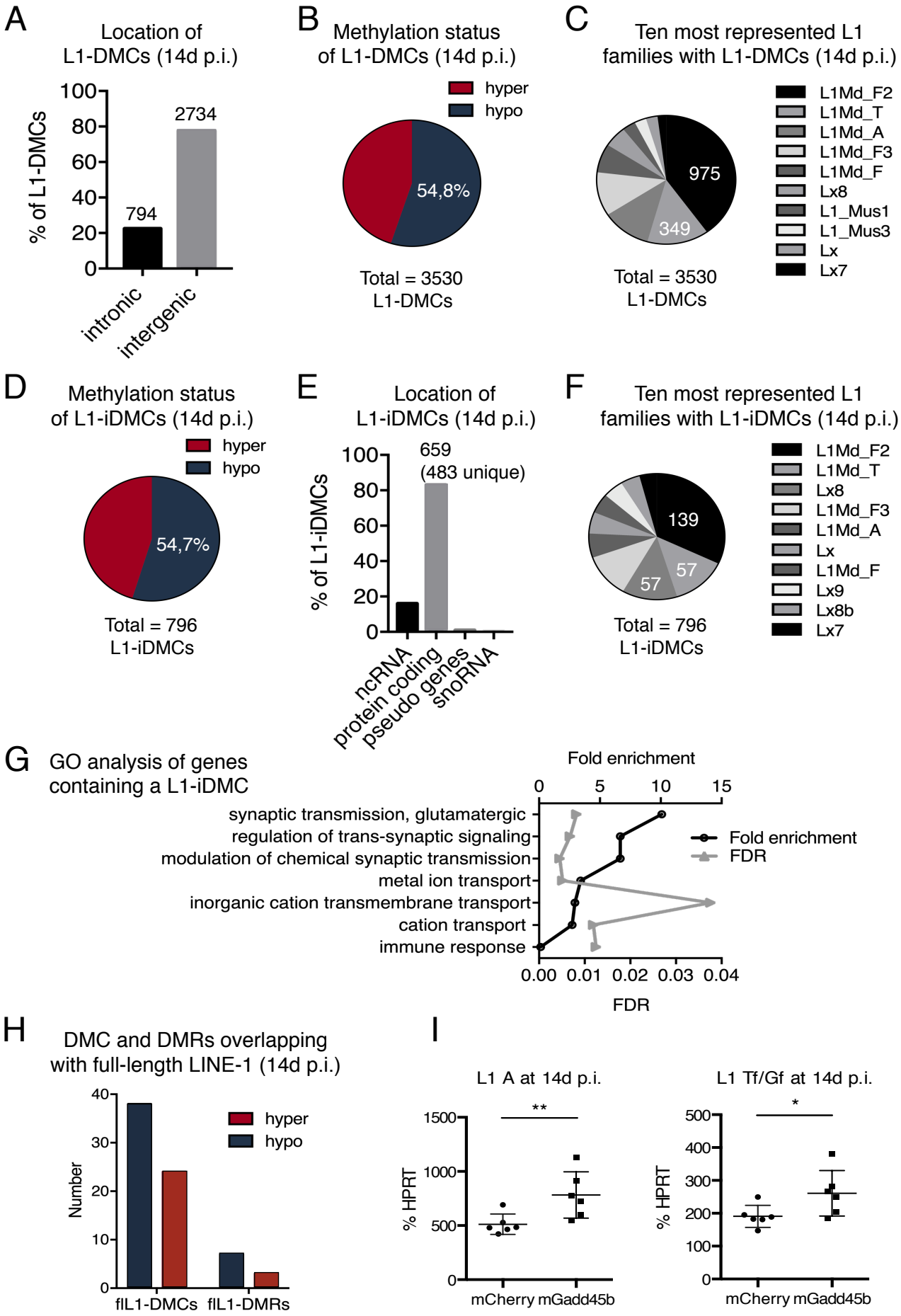
A
Location of
L1-DMCs (14d p.i.)
% of L1-DMCs
100
80
60
40
20
0
794
2734
intronic
intergenic
B
Methylation status
of L1-DMCs (14d p.i.)
hyper
hypo
54,8%
Total = 3530
L1-DMCs
C
Ten most represented L1
families with L1-DMCs (14d p.i.)
975
349
Total = 3530
L1-DMCs
L1Md_F2
L1Md_T
L1Md_A
L1Md_F3
L1Md_F
Lx8
L1_Mus1
L1_Mus3
Lx
Lx7
D
Methylation status
of L1-iDMCs (14d p.i.)
hyper
hypo
54,7%
Total = 796
L1-iDMCs
E
Location of
L1-iDMCs (14d p.i.)
% of L1-iDMCs
100
80
60
40
20
0
659
(483 unique)
ncRNA
protein coding
pseudo genes
snoRNA
F
Ten most represented L1
families with L1-iDMCs (14d p.i.)
139
57
57
Total = 796
L1-iDMCs
L1Md_F2
L1Md_T
Lx8
L1Md_F3
L1Md_A
Lx
L1Md_F
Lx9
Lx8b
Lx7
G
GO analysis of genes
containing a L1-iDMC
Fold enrichment
0
5
10
15
synaptic transmission, glutamatergic
regulation of trans-synaptic signaling
modulation of chemical synaptic transmission
metal ion transport
inorganic cation transmembrane transport
cation transport
immune response
Fold enrichment
FDR
0.00
0.01
0.02
0.03
0.04
FDR
H
DMC and DMRs overlapping
with full-length LINE-1 (14d p.i.)
Number
40
30
20
10
0
hyper
hypo
fIL1-DMCs
fIL1-DMRs
I
L1 A at 14d p.i.
**
% HPRT
1500
1000
500
0
mCherry
mGadd45b
L1 Tf/Gf at 14d p.i.
*
% HPRT
500
400
300
200
100
0
mCherry
mGadd45b

Fig. 5

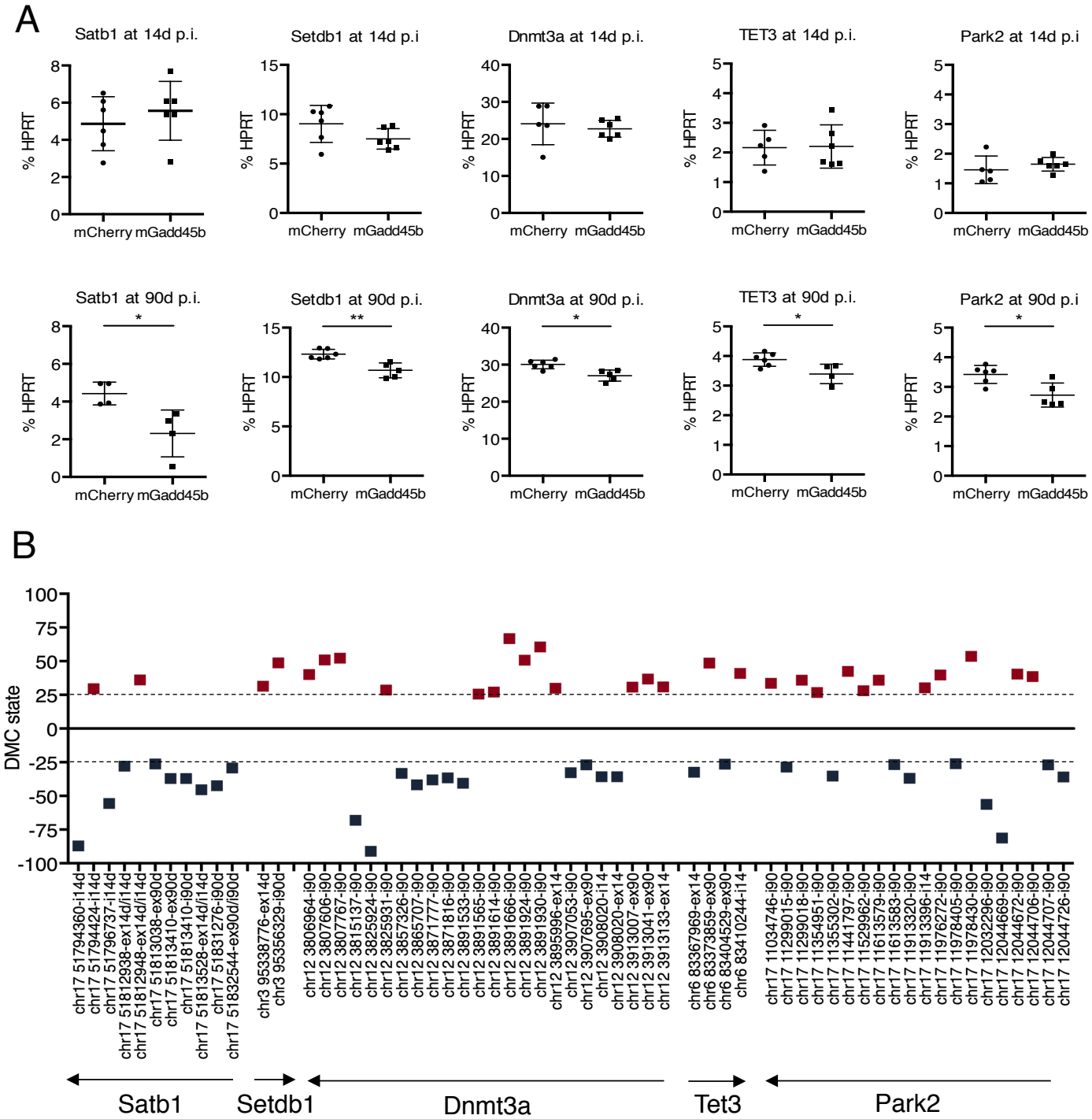
A
Satb1 at 14d p.i.
Setdb1 at 14d p.i
Dnmt3a at 14d p.i.
TET3 at 14d p.i.
Park2 at 14d p.i
Satb1 at 90d p.i.
Setdb1 at 90d p.i.
Dnmt3a at 90d p.i.
TET3 at 90d p.i.
Park2 at 90d p.i
% HPRT
mCherry
mGadd45b
*
**
B
DMC state
Satb1
Setdb1
Dnmt3a
Tet3
Park2

Fig. 6

Differential methylation analysis Gadd45b/ mCherry	**14d p.i.**		**90d p.i.**	
	DMCs	**DMRs**	**DMCs**	**DMRs**
Total number	76185	16702	76639	15685
Hypomethylated (**in %)**	**61,05**	**64,57**	**54,50**	**56,35**
Distance to CpG island (**in %)**				
Islands	15,34	1,50	16,03	1,30
Shelves	4,23	6,30	4,18	6,60
Shores	10,71	7,60	10,73	7,60
Open sea	**69,73**	**84,60**	**69,06**	**84,60**
Association with genomic regions (**in %)**				
Exons	**23,60**	**19,22**	**24,00**	**19,06**
Introns	**41,60**	**45,39**	**41,40**	**45,03**
Promoters	12,50	8,57	12,80	9,03
Intergenic	22,30	26,83	21,90	26,88

Table 1